Development of vanadium based $Li_3V_2(PO_4)_3$ as a potential cathode for Li–ion batteries

A dissertation submitted in partial fulfillment of the requirement for the award of the degree of

MASTER OF TECHNOLOGY

In

NANO SCIENCE AND TECHNOLOGY

By

JITENDRA SINGH

(2K14/NST/04)

Under the Guidance of

Dr. Amrish K. Panwar

Assistant Professor

DEPARTMENTNT OF APPLIED PHYSICS

DELHI TECHNOLOGY UNIVERSITY

BAWANA ROAD, DELHI – 110042

JUNE - 2016

दिल्ली प्रोद्योगिकी विश्वविद्यालय
DELHI TECHNOLOGICAL UNIVERSITY
(Formerly Delhi College of Engineering)

CERTIFICATE

This is to certify that the dissertation entitled on **"Development of vanadium based $Li_3V_2(PO_4)_3$ as a potential cathode for Li–ion batteries"** submitted to Delhi Technological University (formerly Delhi College of Engineering) by **Mr. Jitendra Singh (2K14/NST/04)** in the partial fulfillment of the requirements for the award of the degree of **Master of Technology** in **Nano Science and Technology (Applied Physics Department)** is a bona fide record of the candidate's own work carried out under the supervision of **Dr. Amrish K. Panwar**. The information and data enclosed in this thesis is original and has not been submitted elsewhere for honoring any other degree.

Signature of the Candidate

This is to certify that the above statement made by the candidate is correct to the best of my knowledge.

Signature of the Supervisor

Dr. Amrish K. Panwar
(Assistant Professor)
Applied Physics Department
Delhi Technological University
Delhi - 110042

Signature of the HOD

Prof. S. C. Sharma
(Head of Department)
Applied Physics Department
Delhi Technological University
Delhi - 110042

Candidate Declaration

I hereby declare that the work which is being presented in this thesis entitled **"Development of vanadium based $Li_3V_2(PO_4)_3$ as a potential cathode for Li–ion batteries"** is my own work carried out under the guidance of **Dr. Amrish K. Panwar**, Assistant Professor, Department of Applied Physics, Delhi Technological University, Delhi.

I further declare that the matter embodied in this thesis has not been submitted for the award of any other degree or diploma.

Date: **Jitendra Singh**

Place: New Delhi **Roll No. -2K14/NST/04**

Acknowledgements

With a great pleasure I would like to express my first and sincere gratitude to my supervisor **Dr. Amrish K. Panwar** for his continuous support, patience, motivating ideas, enthusiasm and immense knowledge. His guidance always enlightens and helped me to shape my work.

Besides my Supervisor, I would like to express my deep gratitude and respect to **Prof. S. C. Sharma**, Head, Department of applied Physics, Delhi Technological University, Delhi for his encouragement, insightful comments and valuable suggestions during the course.

I wish to express my heart full thanks to **Mr. Rakesh Saroha, Mr. Aditya Jain** and my friends **Vishwesh Shukla, Sachin Dua and Sandip Verma** for their goodwill and support that helped me a lot in successful completion of this project. I also wish to express my heart full thanks to the classmates as well as staff at Department of Applied Physics, Delhi Technological University, Delhi for their goodwill and support that helped me a lot in successful completion of this project.

Finally, I want to thank my parents, brother and friends for always believing in my abilities and for always showering their invaluable love and support.

Jitendra Singh
M. Tech. NST
2K14/NST/04

ABSTRACT

Li-ion batteries have an unmatchable combination of high power density and energy, making it the technology of choice for portable electronics, power tools, and hybrid/full electric vehicles. There are exciting developments in new positive electrode (cathode) materials to replace the $LiCoO_2$ for use in the lithium-ion batteries (LIBs) over the past decade. In this work the preparation of $Li_3V_2(PO_4)_3$ (LVP) by sol-gel and solid state method with sucrose coating and multi-walled carbon nanotube (MWCNT) doping. The influences of doped MWCNT) and coated sucrose on the physicochemical and electrochemical properties of the as-prepared samples are investigated by X-ray diffraction (XRD), scanning electron microscope (SEM) and electrochemical performances. Doping of 1 wt.% of MWCNT in LVP i.e. LVP/MWCNT and LVP/sucrose shows the proper phase formation of LVP as monoclinic structure. The SEM shows the irregular shape of fine particles and slightly agglomerated particles of average size of range from 1–3 μm in case of MWCNT doped, while 4–6 μm in case of sucrose coated LVP. When charge/discharge at 0.1 C, the samples attain the maximum discharge capacity 90 mAh/g and 100 mAh/g in case of LVP doped with MWCNT and coated with sucrose respectively. Comparing with the sample obtained by LVP/sucrose by sol- gel route, the LVP/MWCNT material displays higher charge transfer resistance, higher rate capability and excellent reversibility. The above experiments demonstrate that the LVP/MWCNT is a very promising cathode material which will be used in the future for lithium-ion batteries.

List of Publications/Communicated in Journal/Conference

1. "Development and Electrochemical performance of alternate cathode, $Li_3V_2(PO_4)_3$/C and Ti based anode, $Li_4Ti_5O_{12}$/C materials for lithium-ion battery", **Jitendra Singh**, Sandip Verma, Rakesh Saroha, Aditya Jain, Amrish K. Panwar, Abstract accepted in 15th Asian conference on solid state Ionics (ACSSI-2k16) @ IIT Patna

Table of Contents

List of Figures

List of Table

Chapter 1

Introduction

1.1 History of Battery

The term “Battery” was firstly used by a U.S. polymath Benjamin Franklin in 1749. At that time battery was used to explain a set of linked capacitors **[1]**. In 1800 Alessandro Volta discovered the first model of battery that was known as voltaic pile. It consisted of a series of Copper and Zinc discs piled which is separated by a cardboard saturated in electrolyte. Volta had done numerous experiments with different types of metals and lastly found that zinc and silver gave the best result. Volta’s pile had some technical faults such as electrolyte leaking, shorts circuits etc. A basic model of Zinc–Copper voltaic pile is shown in figure 1.1

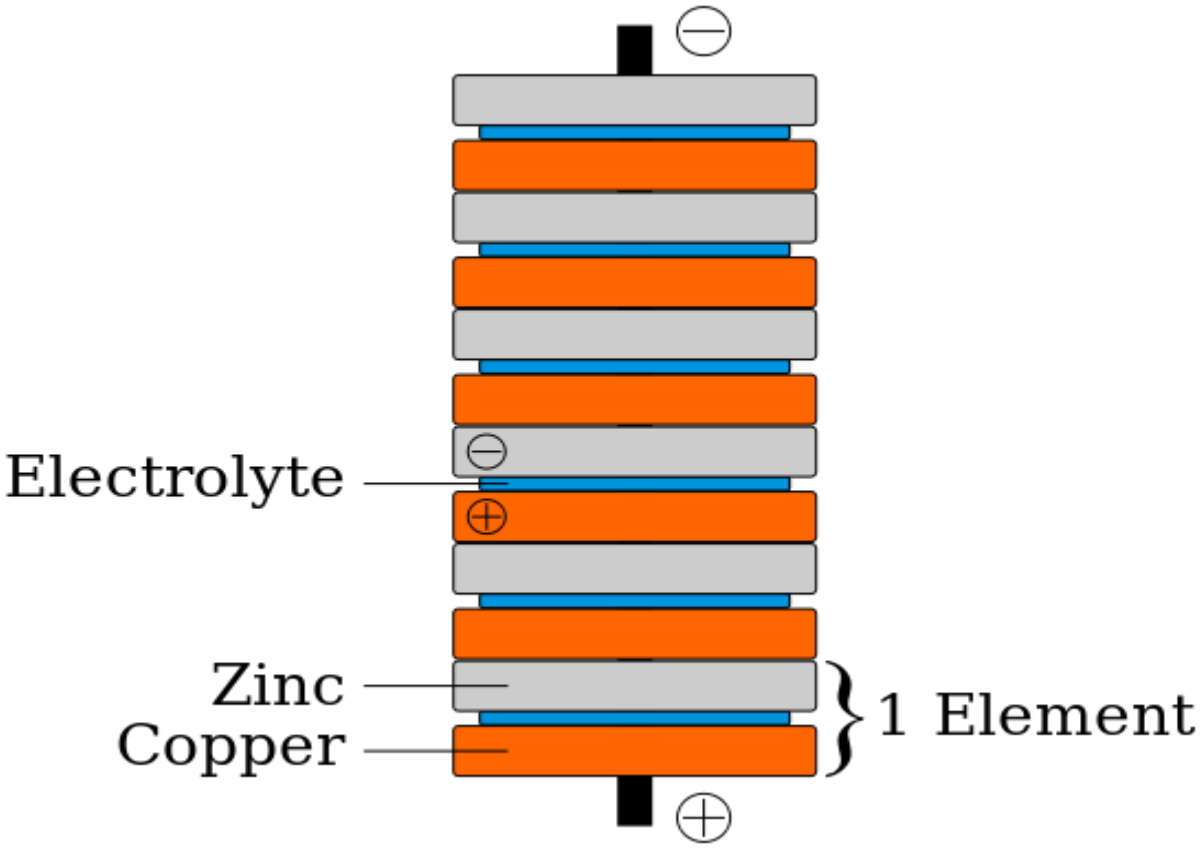

Fig 1.1 A Zinc–Copper voltaic pile [2]

Daniel cell was invented after four decades of volta cell which has given better result than Volta cell and also eliminated many faults of voltaic pile. As the time passes, advancement in electronics industry and invention of different types of electronic goods has increased therefore requirements of higher electrochemical potential and higher energy increase. The

lithium–ion batteries have much higher energy density and much higher density power than Ni–Cd and Ni–MH batteries. This was main reason for using lithium–ion batteries **[3]**. In 1991-92 Sony Corporation, Japan introduced the concept of first commercial lithium–ion batteries **[4]**. Lithium–ion batteries are used in mobile phones, laptops, iPods and PC because of its small size.

1.2 Battery Definition

Battery is a transducer having one or more cells in which chemical energy is converted into electrical energy and vice versa by using an electrochemical oxidation reduction and this energy is used as source of power. Mainly battery can be classified in two types i.e. Primary Battery and Secondary Battery.

Primary Battery:

This type of battery is a portable voltaic cell in which electrode reaction are irreversible, due to this cells are not rechargeable. Therefore cells can be used only once. Zinc/air, Alkaline MnO_2 are examples of primary batteries.

Secondary Battery:

This type of battery is a portable voltaic cell in which electrode reaction are reversible, due to this cells are rechargeable. Therefore cells can be used many times. Ni-Cd, Lead acid and lithium–ion batteries are example of secondary batteries.

1.3 Lithium–ion Batteries

Lithium–ion batteries are secondary type of batteries which can be charged many times. Lithium–ion batteries have an excellent specific energy, power density, highest cell voltage and excellent cycling capacity. Due to these excellent properties it is used for portable electronics, hybrid/full vehicles, and power tools **[5]**.

The development of lithium–ion batteries mainly depends on the following factors.

1. Battery management system
2. Anode, Cathode and Electrolyte
3. Shape or Geometry of the battery

The most popular available anode material is graphite and Lithium Titanate ($Li_4Ti_5O_{12}$), Li_2Sn_5, Li_3Sb, LiB etc. are other examples of anode material. Cathode materials are layered oxide such as $LiCoO_2$, lithium manganese oxide and lithium iron phosphate and electrolyte is a mixture of organic carbonates such as ethylene carbonate consisting lithium ions

complexes. Cathode materials are most important factors as specific capacity, discharge potential, cycling capacity etc. depends on the cathode materials **[6]**.

Table 1.1 Characteristics and comparison of widely used rechargeable batteries [6]

S. No.	Battery / Parameter	Ni-Cd	Lead Acid	Ni-MH	Li-ion
1	Commercial use	1950	1970	1990	1991
2	Cell Voltage	1.25V	2V	1.25V	3.6V
3	Energy Density (Wh/kg)	45-80	30-50	60-120	110-160
4	Load Current(peak)	20C	5C	5C	>2C
5	Fast Charge Time	1h typical	8-16h	2-4h	2-4h
6	Internal Resistance in mΩ	100 to 200	<100	200 to 300	150 to 250
7	Operating Temperature(discharge only)	-40 to 60°C	-20 to 60°C	-20 to 60°C	-20 to 60°C
8	Cycle Life	2000	500-800	500-1000	400-1200
9	Maintenance Requirement	30 to 60 days	3 to 6 months	60 to 90 days	not req.

1.3.2 Construction

Lithium-ion cell consisted of four layer structure. Cathode or a positive electrode which is made from $LiCoO_2$ has a current collector made from thin Aluminium foil. Anode or negative electrode made from carbon having current collector of thin copper foil. A separator made from fine porous polymer film. An electrolyte is formed with lithium salt in an organic solvent **[7]**.

The first generation Lithium- ion battery is shown in figure 1.2 in which $LiCoO_2$ is taken as cathode material, organic solvent of $LiPF_6$ as an electrolyte and graphite as an anode material **[8-10]**.

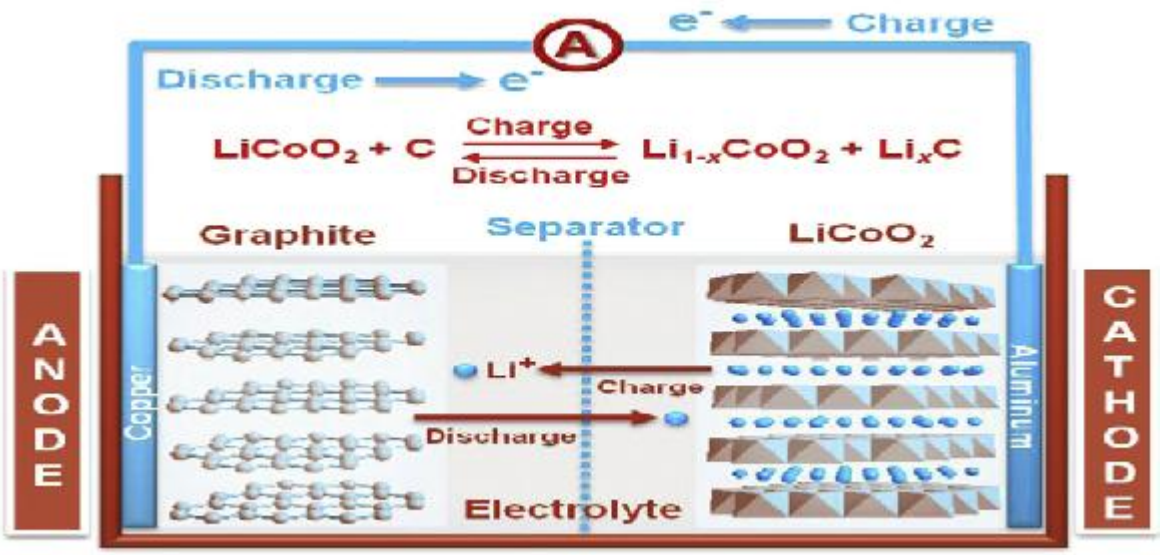

Fig 1.2 Schematic diagram of lithium-ion battery [8]

1.3.3 Principle

While charging the battery, lithium positive ions Li^+ move from cathode terminal to anode terminal through electrolyte and electrons move in opposite directions around the external circuit. When there is no movement of ions it means battery is fully charged and can be used. While discharging the battery ions move from anode terminal to cathode terminal. It means lithium ions are dissociated from anode and they transfer across the electrolyte and inserted into the cathode. Because of charging and discharging, lithium–ion batteries are also known as Rocking chair, swing cells. Figure 1.3 shows the charging and discharging process in a lithium-ion battery **[8].**

At anode: $6C + Li^+ + e^- \Longleftrightarrow LiC_6$

At cathode: $LiCoO_2 - Li^+ - e^- \Longleftrightarrow Li_{0.5}CoO_2$

Overall: $C + LiCoO_2 \Longleftrightarrow LiC_6 + Li_{0.5}CoO_2$

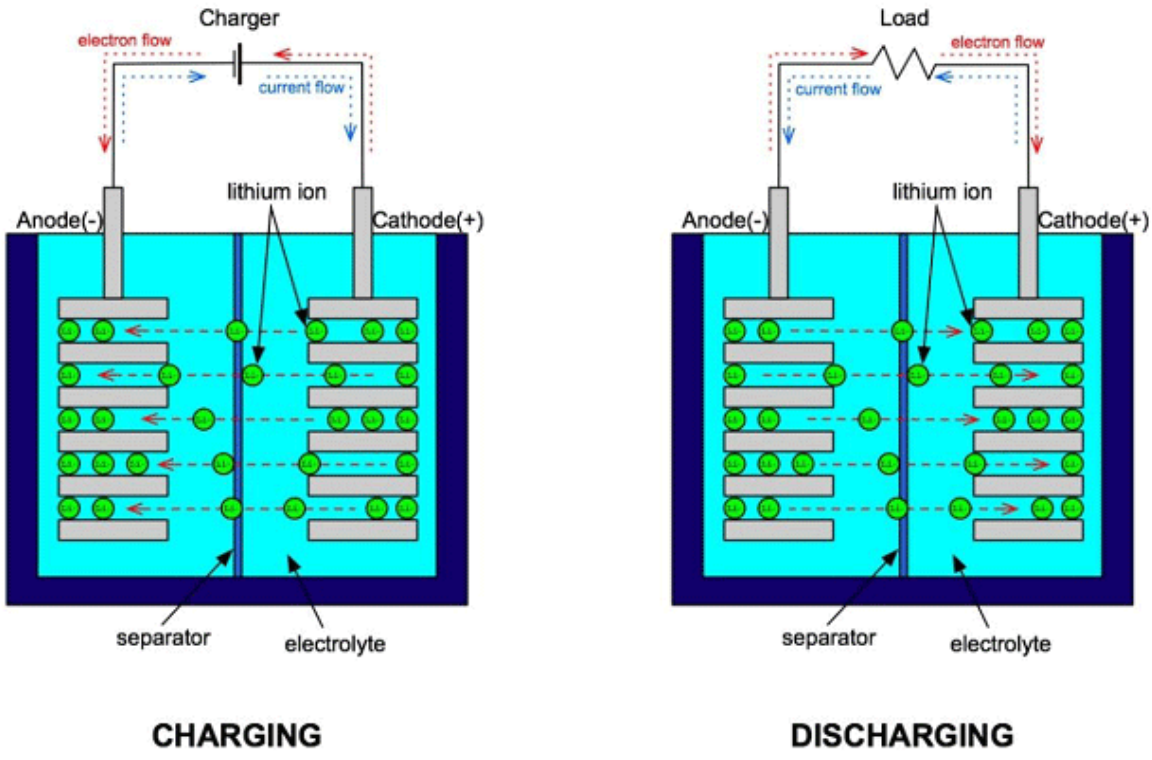

Fig 1.3: Lithium-ion battery (Charging and Discharging) [11]

1.4 Cause of using Lithium-ion battery

Due to enhancement in technology, environment and toxicity based issue become the important areas of concern because such types of factors are basically related to advancement in technology. The following reasons are responsible for using Lithium-ion battery.

- Lithium is lightest metallic element.
- Lithium ion battery is environmentally friendly.
- No problem of toxicity.
- Very high operating potential.
- Lithium ion batteries are light in weight and compact.
- Lithium ion batteries have very high energy density.
- No memory effect.
- Charging of Lithium ion battery is very fast.

1.5 Limitations

Lithium ion batteries have following limitations.

- Problem of short circuiting while transportation.
- Problem of ageing.
- Not cost effective.
- Requirement of protection circuitry i.e. kept within safe operating limits.

1.6 Objective

As well established cathode material $LiCoO_2$ is hazardous in nature and toxic so in place of this existing cathode material, an alternate cathode material is essentially to be replaced in lithium-ion batteries. The aim of this study is synthesis of $Li_3V_2(PO_4)_3$ as alternate cathode material by two different routes i.e. sol-gel and solid state reaction method and to characterize the physio-chemical and electrochemical properties of synthesized materials. The phase formation of $Li_3V_2(PO_4)_3$ with these two synthesis routes has been confirmed by XRD results and further elemental stoichiometric and morphological analysis will be performed by EDS and SEM. FTIR and optical study will be performed to analyze different vibrational modes of as-synthesized LVP/sucrose or LVP/MWCNT or electronic conductivity of synthesized materials will be carried out by LCR meter. Finally, electrochemical performance and electrochemical impedance spectra will be observed for synthesized LVP compounds.

Chapter 2

Literature Review

2.1 $Li_3V_2(PO_4)_3$ or LVP as a cathode material

Lithium is an alkaline metal having silver white in colour. Lithium has large specific capacity (3860 Ah/Kg), low density (0.534 g/cm^3), high energy density (0.9-2.63 MJ/L), High electrochemical potential (-3.05 V), low density (0.534 g/cm^3), high electro negativity **[12]** and soft in handling. $Li_3V_2(PO_4)_3$ or LVP has a high lithium intercalation voltage (~ 3.8V relative to lithium metal) **[13]**, high theoretical capacity (197 mAhg^{-1}) **[14]**, stable with common organic electrolyte and easy with synthesis. Because of above excellent properties, LVP is used as a cathode material for lithium-ion batteries. Comparison of operating voltage and practical capacity of different types of cathode materials used in lithium ion batteries are shown in figure 2.1

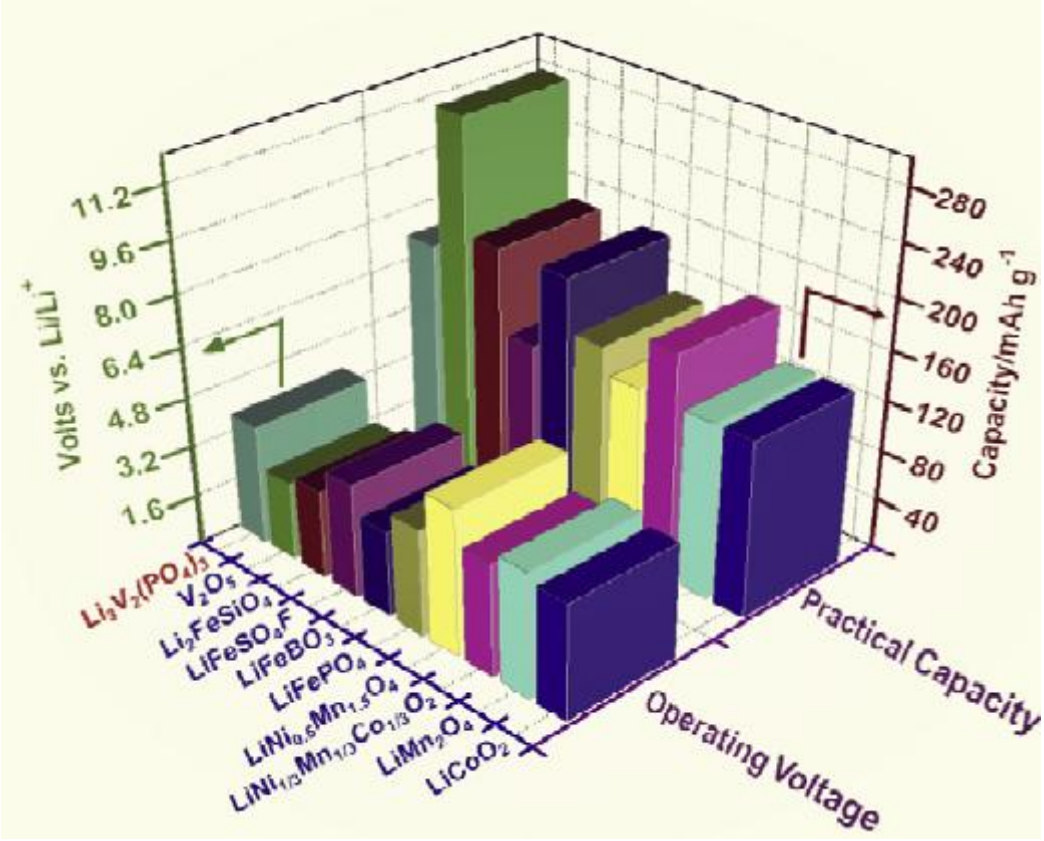

Fig. 2.1 Comparison of operating voltage and practical capacity of different types of cathode materials [15]

2.2 Structure

There are two different frameworks of LVP: Sodium super sonic Conductor (NASICON) or rhombohedral **[16-18]** and monoclinic phase **[19]**. Monoclinic phase is thermodynamically more stable than NASICON phase differing by interconnection of "lantern" units $[V_2(PO_4)_3]$. The NASICON phase of LVP is shown in figure 2.2A, having PO_4 tetrahedra and VO_6 octahedra are joined with their vertices, a formed "lantern" units $[V_2(PO_4)_3]$ is stacked along the direction [001]. Lithium is situated on a unique or distinctive four- fold coordinated crystallographic site **[20]**.

The monoclinic phase of LVP is very similar to NASICON phase in crystallographic way but monoclinic phase is little bit denser than NASICON phase. The three dimensional structure is made from slightly distorted PO_4 tetrahedra and VO_6 octahedra consisting oxygen vertexes **[19, 21-23]** shown in figure 2.2B. Monoclinic phase has two vanadium site V(1) and V(2) having average V-O bond length of 2.003 and 2.006 Å **[19]**. Lithium atoms settled three definite crystallographic site in the interstitial voids. According to solid state nuclear magnetic resonance (NMR) spectrum, Li(1) is located in tetrahedral site while Li(2) and Li(3) are resided in two pseudo tetrahedral sites having an extra long Li-O bond 2.6 Å. Mobility of three lithium site can be calculated by two dimensional exchange spectroscopy (2D EXSY).

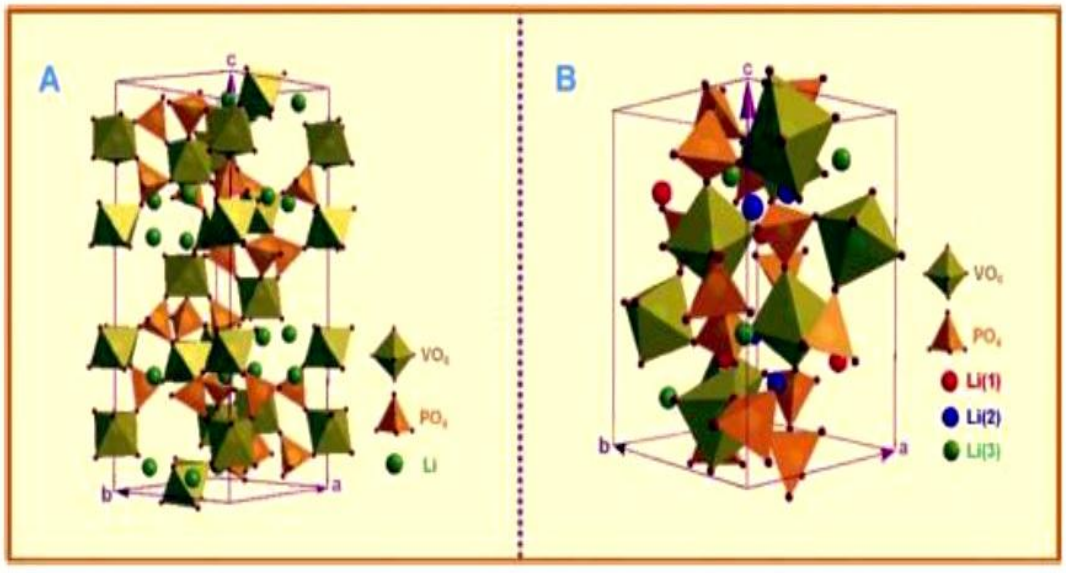

Fig.2.2 Structure of $Li_3V_2(PO_4)_3$ rhombohedral (A) and monoclinic (B) [19]

2.3 Mechanism of charging and discharging

The monoclinic LVP and rhombohedral LVP show very different voltage composition curves because of their structural differences. The rhombohedral LVP simply accessible by ion exchange from the corresponding sodium analog ($Na_3V_2(PO_4)_3$), shows one voltage plateau around 3.70 V vs. Li/Li^+ based on the V^{3+}/V^{4+} redox reaction. In monoclinic LVP all three lithium sites are mobile so have excellent electrochemical properties than rhombohedral. So our main focus on monoclinic LVP. The electrochemical voltage composition curve of lithium extraction and reinsertion in LVP are shown in figure 2.3 A for the voltage range of 3.0-4.8 V vs. Li/Li^+ and for the voltage range of 3.0-4.3 V vs. Li/Li^+ in figure 2.3 B which is given below.

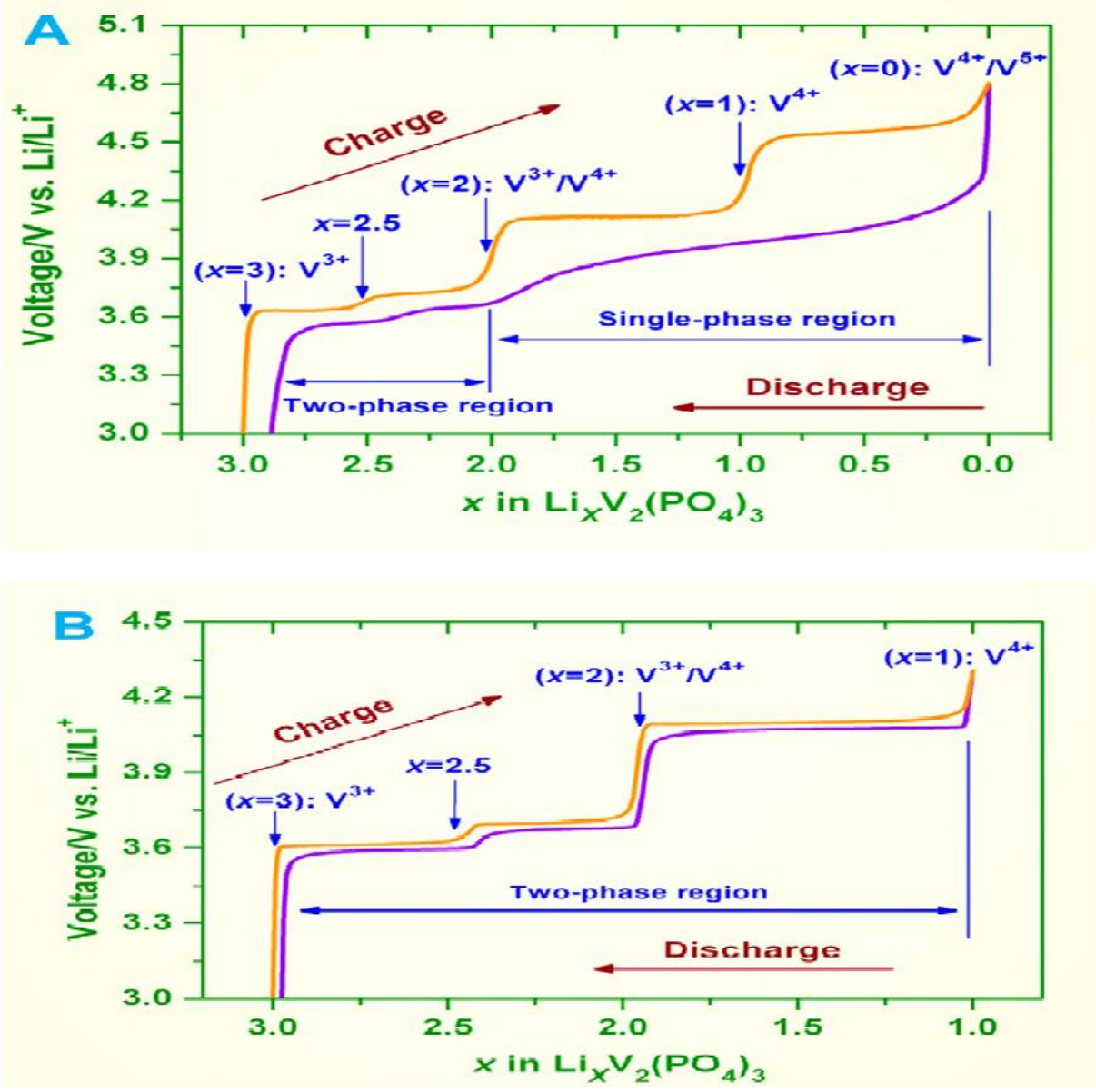

Fig. 2.3.The electrochemical voltage composition curves of $Li_3V_2(PO_4)_3$ in the voltage ranges of 3.0-4.8 V(A) and 3.0-4.3 V vs. Li/Li^+ (B) [24]

In the voltage range 3.0-4.3 V vs. Li/Li^+, more stable capacity retention can be seen for LVP **[24-26]**. The overall electrochemical reaction is given below **[24]**.

Charge:

$$Li_3V_2^{3+}(PO_4)_3 - 0.5Li^+ - 0.5e^- \longrightarrow Li_{2.5}V^{3+}V_{½}^{4+}(PO_4)_3 \quad (1)$$

$$Li_{2.5}V^{3+}V_{½}^{4+}(PO_4)_3 - 0.5Li^+ - 0.5e^- \longrightarrow Li_2V^{3+}V^{4+}(PO_4)_3 \quad (2)$$

$$Li_2V^{3+}V^{4+}(PO_4)_3 - Li^+ - e^- \longrightarrow LiV_2^{4+}(PO_4)_3 \quad (3)$$

$$LiV_2^{4+}(PO_4)_3 - Li^+ - e^- \longrightarrow V_2^{4.5+}(PO_4)_3 \quad (4)$$

Discharge:

$$V_2^{4.5+}(PO_4)_3 + 2Li^+ + 2e^- \longrightarrow Li_2V^{3+}V^{4+}(PO_4)_3 \quad (5)$$

$$Li_2V^{3+}V^{4+}(PO_4)_3 + 0.5Li^+ + 0.5e^- \longrightarrow Li_{2.5}V^{3+}V_{½}^{4+}(PO_4)_3 \quad (6)$$

$$Li_{2.5}V^{3+}V_{½}^{4+}(PO_4) + 0.5Li^+ + 0.5e^- \longrightarrow Li_3V_2^{3+}(PO_4)_3 \quad (7)$$

2.4 Transport properties

The electrochemical performance of lithium ion battery, rate capabilities, cycle life and capacity mostly depend on the ionic and electronic conductivities of electrode materials. Following transport properties of LVP is given below.

2.4.1 Electronic Conductivity

The pure LVP compound exhibits a comparatively low electronic conductivity (e.g. 2×10^{-8} S/cm) **[19]** and 7.7×10^{-8} S/cm **[27]** are calculated by using four point probe conductivity measurement which is equivalent to other lithium metal phosphate but much less than LCO **[28]**. Conductivity of LVP can be increased by transition metal doping **[29]**, surface coating with carbon **[27, 30]** or a combination of them. By using such doping, an extraordinary increment in electronic conductivities have been attained e.g. 7.2×10^{-5} S/cm for LVP/C **[27]**.

2.4.2 Lithium Diffusion

The charging and discharging rate capabilities of high power lithium ion battery application is largely analogous to lithium ion diffusivity. Higher diffusivity leads to a faster lithium insertion or extraction rate. The migration energies for lithium ion diffusion has been calculated by Lee et al. along the different direction of LVP on basis of vacancy hopping mechanism based on Mott-Littleton **[31]**. The probable Li^+ migrations pathway in LVP has been shown in figure 2.3 **[31]**.

In crystalline solid electrode, lithium diffusion can be calculated by electrochemical impedance spectroscopy (EIS), electrochemical technique of cyclic voltammetry (CV) and galvanostatic intermittent titration techniques (GITT) at macroscopic level **[32-34]**. The low ionic and electronic conductivity of LVP will lead to slow kinetic of charge and discharge, generating poor rate capacity. Thus the improvement of lithium diffusion and electronic conductivities has been becoming core area of LVP study.

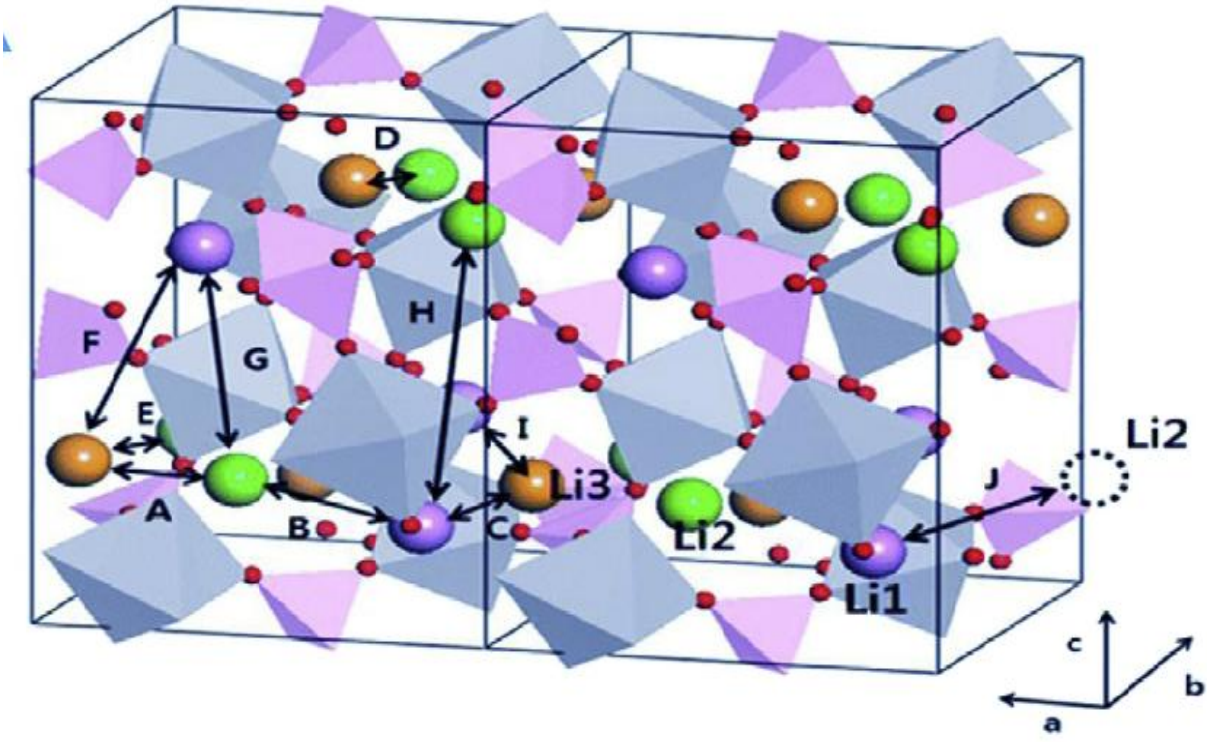

Fig. 2.3 The probable Li^+ migration pathway in LVP [31]

2.5 Various synthesis methods

The charging and discharging capacity and cyclic performance of LVP has been mostly affected by various synthesis methods and conditions. The conventional synthesis methods are sol-gel method, solid state method, carbothermal reduction method, microwave assisted method, hydrothermal method, spray pyrolysis, electrostatic spray deposition method and so forth. Some of above these methods are explained below.

2.5.1 Sol-gel method [35-36]:

Dispersion of colloidal particles in the liquid state is known as sols. Gels can be defined as significantly diluted cross linked system which shows no movement in rest position with pores of sub-micrometre dimensions. The LVP prepared by sol-gel method has fine uniformity with small particle size, high purity, low temperature requirement and the reaction process can be easily control. The main drawback of this method is that this method is not suitable for industrial production.

2.5.2 Solid state method [37]:

Solid state reaction is very common method for preparing ceramic because this method is easy for industrialization and synthesis process is very easy. In this method solid precursor is ball milled or ground followed by heat treatment of the mixture in a furnace. The main drawback of this method is that, prepared product has non-crystalline form, non-uniform particles and the synthesis duration is very high. The sintering temperature has a great effect on the properties of LVP which not only affect the purity of the LVP particle but also affect the discharge capacity of the material. In general, the appropriate sintering temperature range is 700-800 °C. It requires high temperature, high energy, high temperature, long processing time and repeated grinding. As a result, the product cost becomes very high.

2.5.3 Hydrothermal method [38-39]:

The hydrothermal method of synthesis of LVP is performed in autoclave. This method is carried out in aqueous medium so it requires very precise control of temperature and pressure. This method is suitable for the preparation of fine particles. The advantage of this method is that, simple synthesis process, homogeneous products, fast reaction kinetics and a well control morphology. This method has become an important method for the synthesis of different types of electrode materials for lithium ion battery.

2.5.4 Spray pyrolysis method [40-41]:

Spray pyrolysis method is very efficient method for producing excellent quality of ceramic particles with pure crystallized phase in a single phase within a short time. Apart from this, this method has a potential to generate high purity, spherical morphology, chemically homogeneous powder of fine size and non agglomerated particles. Spray pyrolysis method is composed of a quartz reactor, a powder collector and a droplet generation. Droplets were carried into high temperature tubular reactor using carrier gas. After this powder and droplets were evaporated, decomposed and crystallized in the quartz reactor. It is the appropriate method for synthesizing spherical LVP.

2.6 Various approaches for improving electrochemical performance

Various methods are given below for improving electrochemical performance of LVP.

2.6.1 Doping

Ion-doping is an effective method for improving Li-ion diffusion and the intrinsic electronic conductivity. The advantages of ion-doping on the, cycle life, rate capability and capacity delivery of LVP has been demonstrated by many research groups **[42-44]**. Supervalent cations such as Mn^{2+}**[45]**, Co^{2+}**[46]**, Ni^{2+}**[47]**, Fe^{3+}**[48]** etc. have been used as dopant in LVP. Anion doping **[49]** and multi element doping **[50-51]** have also been used as dopant in LVP system.

2.6.2 Carbon coating

Coating of surface of LVP particles with amorphous carbon is the best method for improving its electronic conductivity therefore active material can be substantially used at high current rate. During high temperature calcinations, aggregation and growing up of LVP particles can be reduced by carbon coating. Carbon source material can act as chelating agent as well as reducing agent for reducing V^{5+} to V^{3+}.

Table 2.1 effect of carbon coating on electrochemical performance of LVP

Carbon source	Content	Preparation method	Electrochemical performance	References
Sucrose	5 wt%	Hydrothermal	In voltage range 3.0 to 4.8 V, 145 $mAhg^{-1}$ for first cycle at 0.1C	**[52]**
Glucose	4.8 wt%	Sol gel and Hydrothermal	In voltage range 3.0 to 4.5 V, 127.8 $mAhg^{-1}$ initial capacity with capacity retention of 98.5% after 50 cycle at 0.2C	**[53]**
PVA 2000	3.1 wt%	Sol gel	In voltage range 3.0 to 4.3 V, 100 $mAhg^{-1}$ reversible capacity at 1C	**[54]**
Citric acid	1.57 - 4.56 wt %	Sol gel	In voltage range 3.0 to 4.3 V, 117$mAhg^{-1}$ during 150 cycle at 10C	**[55]**
Citric acid	3.98 wt %	Freeze drying	In voltage range 3.0 to 4.8 V, 1110.8 $mAhg^{-1}$ at 5C	**[56]**
Citric acid	4.1 wt%	Spray drying	In voltage range 2.5 to 4.5 V, 161.3 $mAhg^{-1}$ at 0.1C	**[57]**
Starch	3.45 wt%	CTR	In voltage range 3.0 to 4.3 V, 130 $mAhg^{-1}$ at 0.1C	**[58]**
Maleic acid	3.3 – 5.8 wt%	Sol gel	In voltage range 3.0 to 4.8 V, 179.8 $mAhg^{-1}$ at 0.1C	**[59]**
CMC	3.3 wt%		In voltage range 3.0 to 4.8 V, 172 $mAhg^{-1}$ for first cycle at 0.1C	**[60]**

2.6.3 CNT or Graphene doping

Electronic conductivity of LVP can be enhanced by doping of CNT or graphene.

Chapter 3

Experimental Procedure

3.1 Synthesis of LVP by Sol- gel method

In the first step all the starting material are mixed thoroughly in stoichiometric ratio as 3.0606 gm of CH_3 COOLi, 1.818 gm of V_2O_5, 3.9618 gm of $(NH_4)_2HPO_4$ and 0.44206 gm of sucrose (5 wt.%) are mixed thoroughly by grinding in an pestle and mortar and then dissolved in deionized water for ultrasonic treatment.

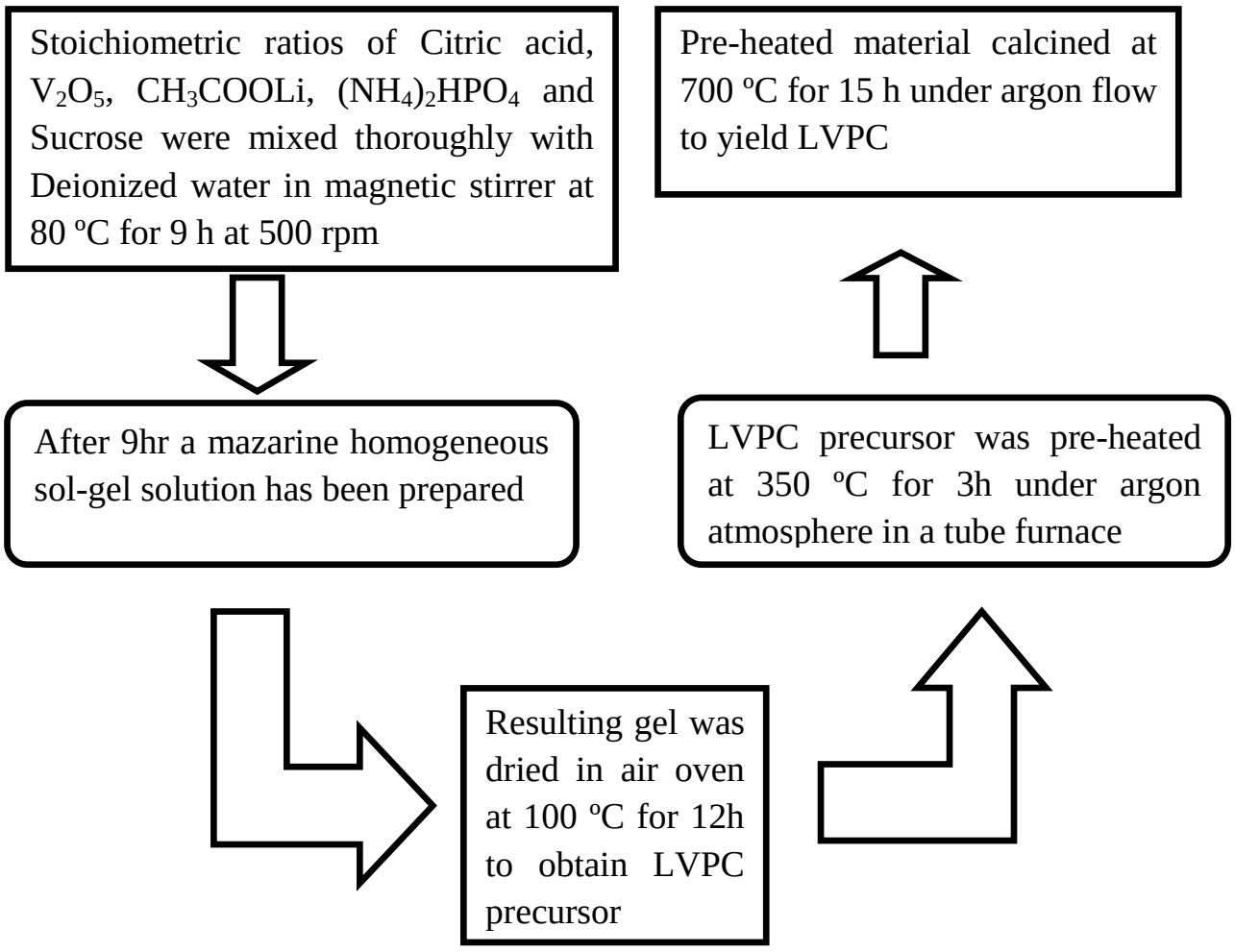

Fig 3.1 Block diagram of synthesis of LVP/sucrose by Sol gel method

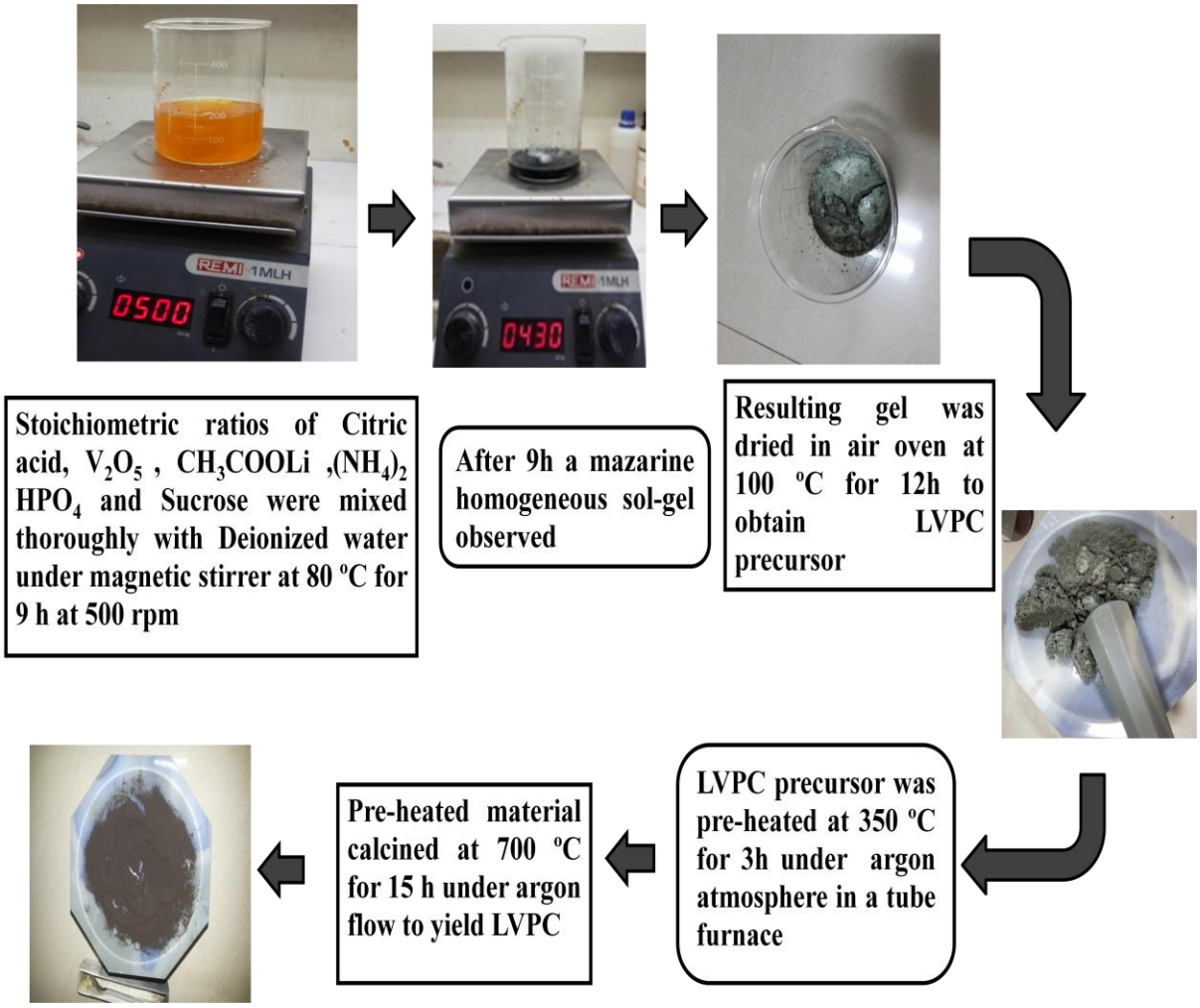

Fig 3.2 Systematic illustration of synthesis of LVP/sucrose via sol-gel route

Secondly, 4.3123 gm of a saturated citric acid solution was added drop wise into mixed solution under magnetic stirrer. After that, the mixed solution was mildly heated with continuous stirred to evaporate the excess water at 80 ^{o}C at 500 rpm for 9 h, and mazarine homogeneous sol became gel. The resulting gel was dried in an air oven at 100 ^{o}C for 12 h to obtain LVPC precursor. Further, the LVPC precursor was pre-heated at 350 ^{o}C for 3 h under argon atmosphere in a tube furnace and then cooled to room temperature. Then, the pre-heated material was calcined at temperatures 700 ^{o}C for 15 h under argon flow to yield the LVP/sucrose in sample. Block diagram of experimental procedure is given in figure 3.1

3.2 Synthesis of LVP/MWCNT by solid state method

Experimental procedure is shown in block diagram figure 3.3.

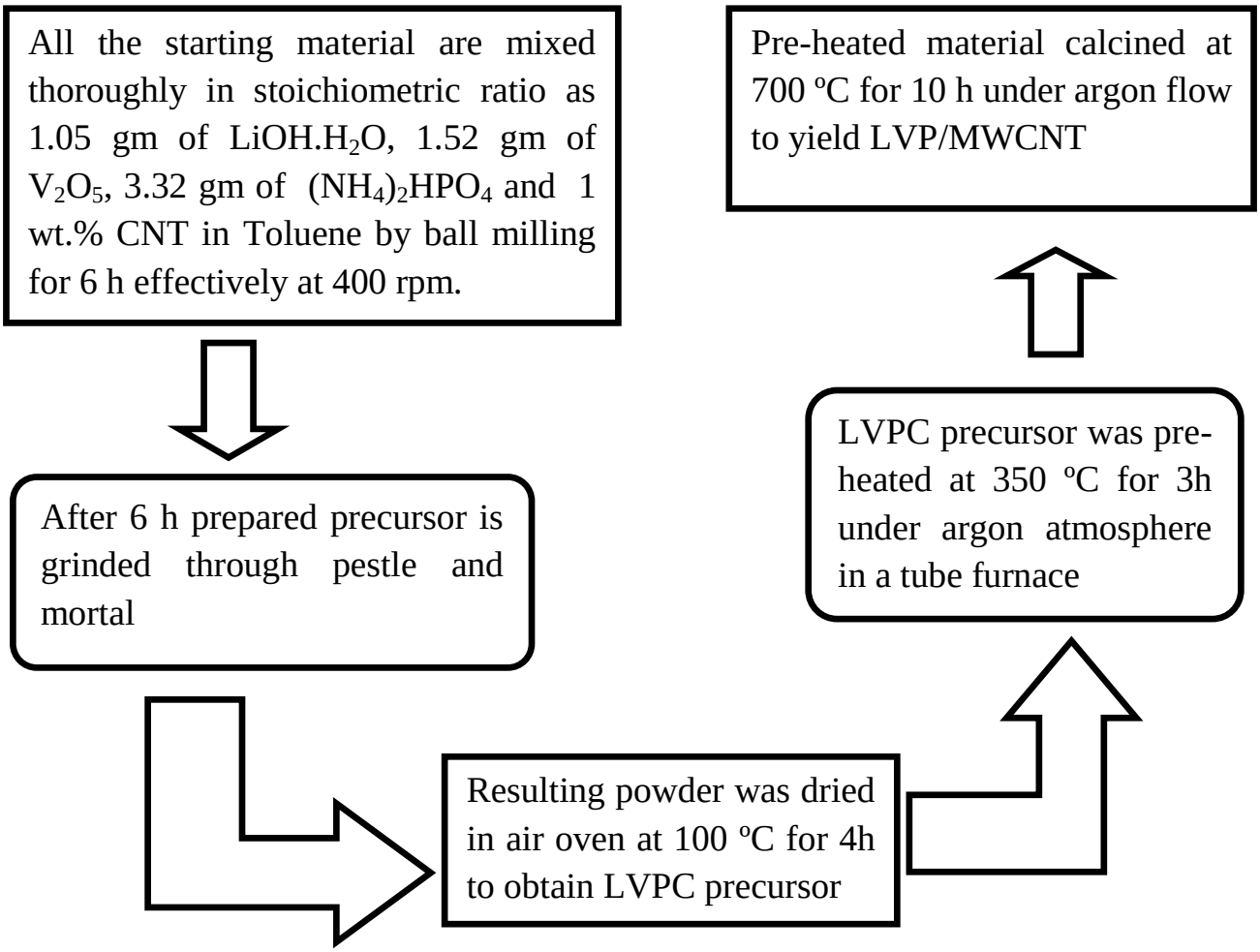

Fig 3.3 Block diagram of synthesis of MWCNT doped LVP by solid state method

3.3 Pellet formation

The calcined powder of LVP obtained from sol-gel or solid state method was mixed with PVA binder. Mixing of 0.5 gm PVA powder in 20 ml of distilled water and after this stirring for 1 h is performed to obtain a thick sticky liquid of binder. Some drops of this solution are added to the LVP powder and again grinding is done in pestle and mortar for some time. Now this mixture is pressed into pellets form using a hydraulic pressing machine applying a pressure about 80 KPa. The pellets are then heated at 120 ^oC for 2 h for removing PVA. These pellets were coated with silver paste to form electrode to measure conductivity of LVP and for removing moisture pellets were again heated in hot air oven at 150 ^oC for 2 h.

3.4 Electrode and coin cell preparation

For electrochemical studies, the electrodes and coin cell preparation of synthesized active material LVP are as follows.

Active material and Super P or Carbon Black were grinded in pestle and mortar up to 45 minutes, Binder Polyvinylidene difluoride (PVDF) and N-methyl pyrrolidinone (NMP) solvent were mixed thoroughly until a transparent solution become. For slurry, Active material, Super P, PVDF and NMP were mixed in the weight ratio 70:15:15 in magnetic stirred for 8 h. Resulting Slurry was coated on Al foil using the Doctor Blade. Then coated sheet was dried at 120 ^{o}C in vacuum oven for overnight to evaporate the solvent. The thickness of coated sheet should be reduce and reduced thickness is given below.

Coated sheet thickness = 45 µm

Al sheet thickness = 17 µm

Difference of coated sheet and Al foil sheet = 28 µm

Required pressing thickness = 45- 10% of 28 = 42.2 µm

Then this coated sheet is passed through rolling machine for reducing the sheet thickness. After rolling the coated sheet, keep it in vacuum oven at 85 ºC for 2 h and using the disc cutter, circular electrodes were punched.

And finally Electrodes were brought inside the Glove box maintained below 0.5 ppm of O_2 and H_2O. For electrochemical testing, the coin cells were assembled in glove box in which a polypropylene as a separator, 1M $LiPF_6$ as salt in EC:DMC in1:1 as electrolyte and Li metal foil were used. After assembling, coin cells were pressed by crimping machine.

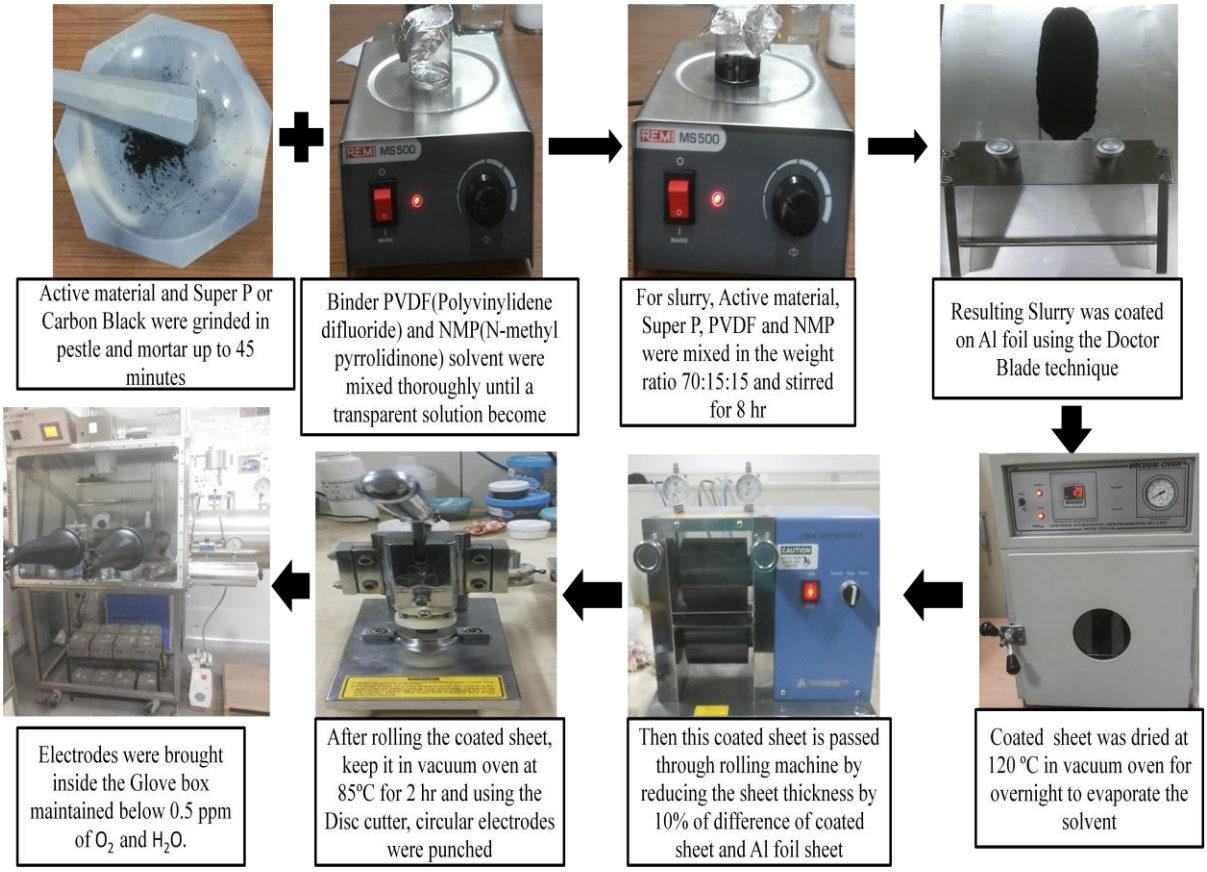

Fig 3.4 Systematic illustration of electrode and coin cell preparation

Chapter 4

Methods of characterization

Characterization techniques refers to those methods which one can easily identify prepared sample with respect to its surface topology, morphology, internal structure, composition, etc. These techniques were used to study the properties, tolerance of a sample to the imposed environment so that during the process, no damage will occur to the sample either internally or externally. Following techniques were adopted for characterization.

4.1 X-ray Powder Diffraction (XRD)

X-ray diffraction technique has been used to get information about phase identification, crystal size of samples and miller planes of unit cell dimensions. It uses the concept of spatial distribution of X-rays radiation scattered by sample and intensities. Crystals constitutes naturally produced diffraction gratings for X-rays and have a solid periodicity in structure. When X-rays colloids with the particles of samples, X-ray are diffracted according to electron and x-ray collision. The structure of sample particle and wavelength of sample effects the pattern of X-ray diffraction.

Crystals are generally regular arrays of atoms in which atoms are periodically arranged. When X-ray waves interacted with the periodic atoms then scattering of wave happened in backward direction. X-ray striking electron will produce secondary spherical waves emerging from electron. This is called as elastic scattering, and the electron is known as the scatterer. A regular arrays of spherical waves is produced by atoms of a sample. The constructive interference of forward and backward wave is responsible for getting the information about XRD which can be calculated by Bragg's law. When X-rays having wavelength λ of the order of magnitude (1–100 Å) and sample's crystal spacing *d* between them will produce the diffraction pattern. According to the Bragg law,

$$2d\sin\theta = n\lambda$$

Where θ is scattering angle and n is an integer.

Where incoming x-ray wavelength (λ) is related to planar distance of the crystal (d) is shown in figure below. XRD is a non-destructive analytical method for identifying orientation as

well as phase, estimate the size of nanoparticles, determine the structural properties and to measure the thickness of thin films,

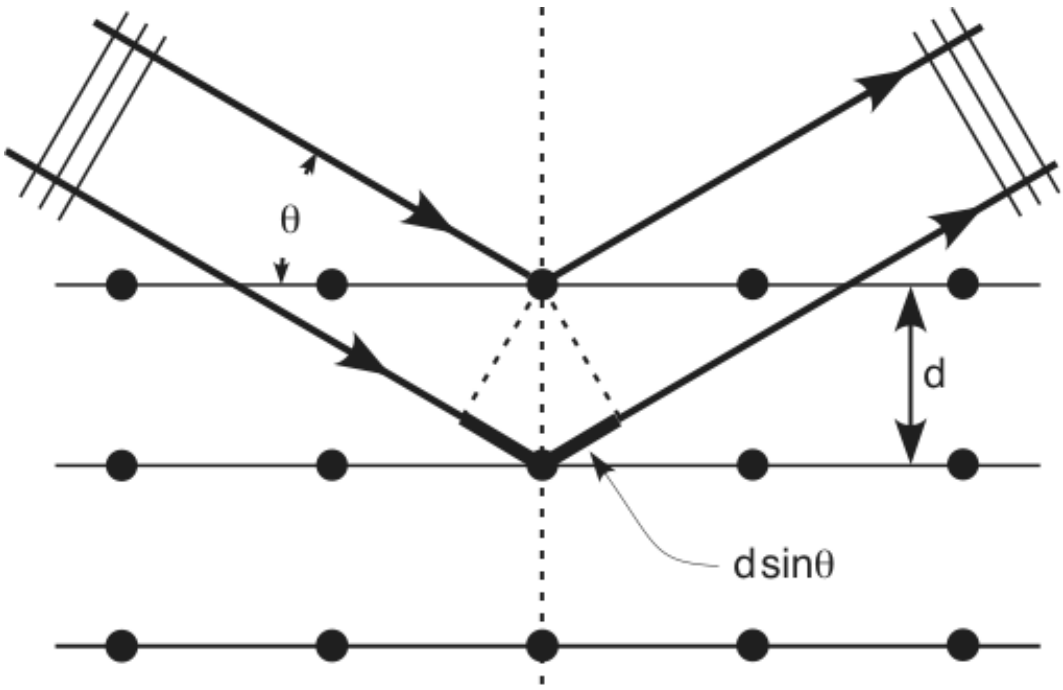

Fig 4.1 Bragg diffraction [61]

Fig 4.2 X-ray diffraction equipment used in the XRD characterization of LVP

4.2 Scanning Electron Microscopy (SEM)

SEM is a type of electron microscopy which creates images of a sample by scanning the sample with the help of focused beam of electrons. It generates different types of signals when electrons interacted with the sample's atom which can be detected and concluded the information about the sample's surface compositions and topography. The electron beam is generally scanned in a raster type scan pattern and to create an image, the position of the beam is merged with the detected signal. The electron beams excited the secondary electrons from the sample surface which is largely detected by SEM. The amounts of secondary electrons depend on the angle at which beam encounters specimen surface, (i.e. on specimen topography). In a SEM, there is a special type of detector which can be used to detect and collect the secondary electron by scanning the sample. Hence an image displaying the topographical details of the surface is created, Showing size and shape of sample having minute characteristics less than 1 nanometre in size.

SEM is typically compromises of the following features

- A source or electron gun of the electron beam which is accelerated down to the column.
- A series of lenses that is objective and condenser which control the diameter of the beam as well as focus of beam on the specimen.
- An area of beam or interaction which produces several kinds of signals that can be detected and processed for creating an image or spectra.
- A series of apertures that is micro scale holes in metal films through which the beam passed and that affects properties of that beam.
- Control for specimen position (x, y, z) as well as orientation (tilt, rotation).
- All the components were maintained at high vacuum levels.

A thermionic electron beam of SEM is emitted from an electron gun which is equipped from a tungsten filament cathode. The electron beams have energy generally of the order of ranging from 0.2 to 40 keV, this beam is pointed by one or two condenser lenses for a spot having the diameter 0.4 nm to 5 nm. Then the beam is passed through pairs of deflector plate or couple of scanning coils existing in electron column, and lastly through deflector lens, that deflects the beam and scan in a raster way to cover a rectangular area in x and y axes of the sample's surface.

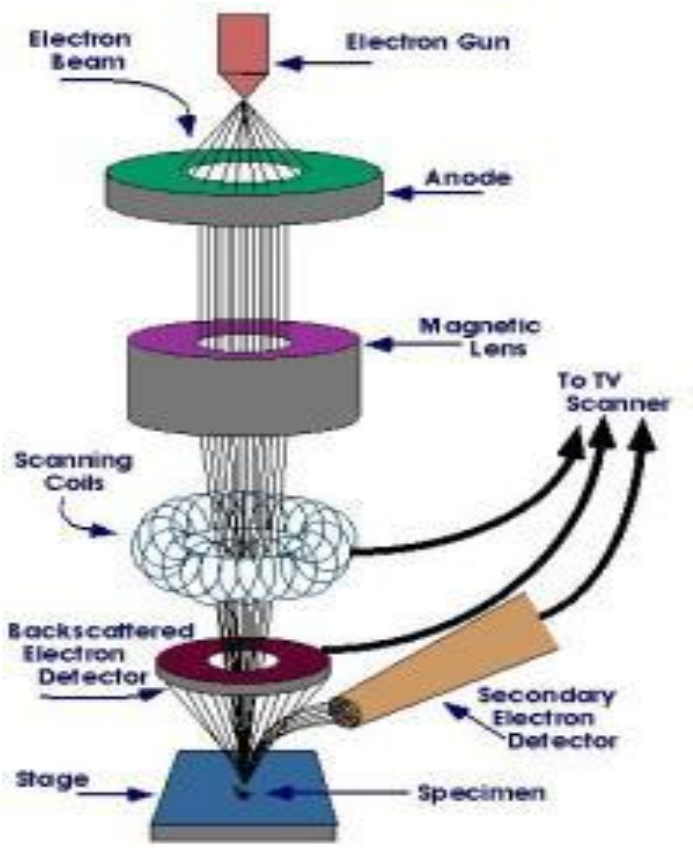

Fig 4.3 Schematic of SEM apparatus [62]

Fig 4.4 Scanning electron microscope equipment used in the SEM characterization of LVP

This process starts from top to bottom and from left to right. Rastering pattern is used to produce the image on monitor screen. The variety of pixels in every row yet as total number of rows of the scanned space was laid low with the resolution selected for image. When primary beam of electrons passing through focusing lenses interact with the sample, the electrons loose their energy by continual random absorption and scattering at intervals the interaction volume, that is generally but 100 nm to 5 μm into the surface. Different types of signals produced by a SEM include secondary electrons (SE), back-scattered electrons (BSE), Auger electrons, characteristic X-rays, and light (cathodoluminescence) (CL).

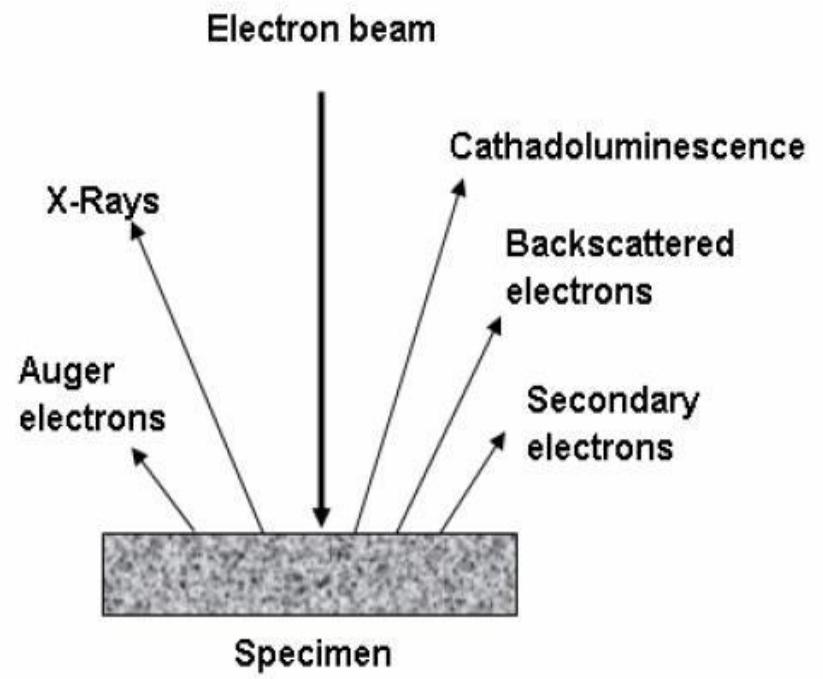

Fig 4.5 Different types of electrons released during SEM imaging [63]

Secondary Electrons:

If an incident electron will collide with an electron in a sample atom, electron will be knocked out from its orbital shell and the atom is converted into ionized form. Multiple collisions are possible because the incident electron loses only a small amount of energy during every collision. Hence, such process continues until the occurrence electron has no additional energy to extricate secondary electrons. Every freed secondary electrons have a small kinetic energy (<50 eV), which is independent from energy of the incident electron.

These secondary electrons can escape from sample and can be collected by the detector. Hence, sample topography can be seen through secondary electron imaging.

Backscattered Electrons

If an electron connects with the core of a surface molecule, then the electron will bob back or disperse "in reverse" out of the specimen as a backscattered electron (BSE). These backscattered electrons have high energies, commonly in the scope of 50 eV. Atomic number of test influences the no of BSE electrons in this way the creation of these BSE electrons changes straightforwardly with atomic no and to recognize contrasts in test atomic number, backscattered electron images can be utilized.

Auger Electrons

A vacancy is created in an ionized atom's electron shell because of generation of secondary electron. In order to fill these vacancies, an electron from a higher energy outer shell state can drop down to fill the vacancy. Because of this surplus energy in the atom, an outer electron is emitted which is known as an Auger electron. Auger electrons are emitted from shallow sample depths (<3 nm) because they have a relatively small kinetic energy. These electrons can be used to provide compositional information about the target sample.

Characteristic X-rays

When an incident electron beam colloids with the sample's surface, X-rays are generated. These excess energy X-rays' is produced as a result of reshuffling electrons to fill shell vacancies same like the Auger electron producing process. X-rays give compositional information about the sample structure because they have a characteristic energy distinctive to the element from which they are emitted.

4.3 FTIR Spectroscopic Analysis

FTIR (Fourier transform Infrared) Analysis is most powerful technique for differentiating chemicals that are either inorganic or organic. It is basically used to quantities some parts of an unknown mixture. It is applied for the analysis of solid, liquids and gasses. FTIR spectroscopic can be a multiplexing technique, where all optical frequencies from the supply are found in the meantime over a measure of time alluded to as sweep time. During this system entire data is gathered and recovered from an interference pattern to a spectrum. FTIR

Spectra of pure compounds are hardly so distinguish that they are sort of a molecular "fingerprint". Whereas organic compounds have extremely rich, elaborated spectra, inorganic compounds are hardly easier. These techniques work on the fact that bonds and groups of bonds should vibrate at characteristic frequencies. A molecule that is presented to infrared beams absorbs infrared vitality at frequencies that are trademark to that atom i.e. those frequencies where the infrared radiation influences the dipolar characteristic of the molecule. So mono atomic (Ar, Ne, He, etc) and homo polar diatomic (H_2, O_2, N_2, etc) molecules do not absorb infrared radiation during FTIR analysis, a position on the specimen has been subjected to a modulated IR beam.

The example's transmission and coefficient of reflection of the infrared beams at very surprising frequencies is interpreted into an IR absorption plot comprising of opposite crests. The following FTIR pattern is then broke down and coordinated with prominent marks of known materials inside the FTIR library. According to Beers Law a relation between IR absorption and transmittance is given below.

$$A = \log_{10} \frac{1}{T} = -\log_{10} T = -\log_{10} \frac{1}{I_0}$$

Where A is Absorbance, T is transmittance which is the relation of radiant power transmitted by the sample (I) to the radiant on the sample (I_0).

The transmission spectra gives highest differences between intensities of strong and weak bands which give transmission ranges from zero to 100% T. whereas absorbance (A) ranges from infinity to zero.

4.4 Multi channel Cycler

Electrochemical impedance spectroscopy (EIS) for impedance measurement using 5 mV an ac voltage in the frequency range 10 mHz to 10 kHz and Galvanostatic charging discharging (GCD) for rate capability at different C- rate have been performed in multi channel cycler. Above these electrochemical tests have been performed using Bio Logic SAS instrument French based company.

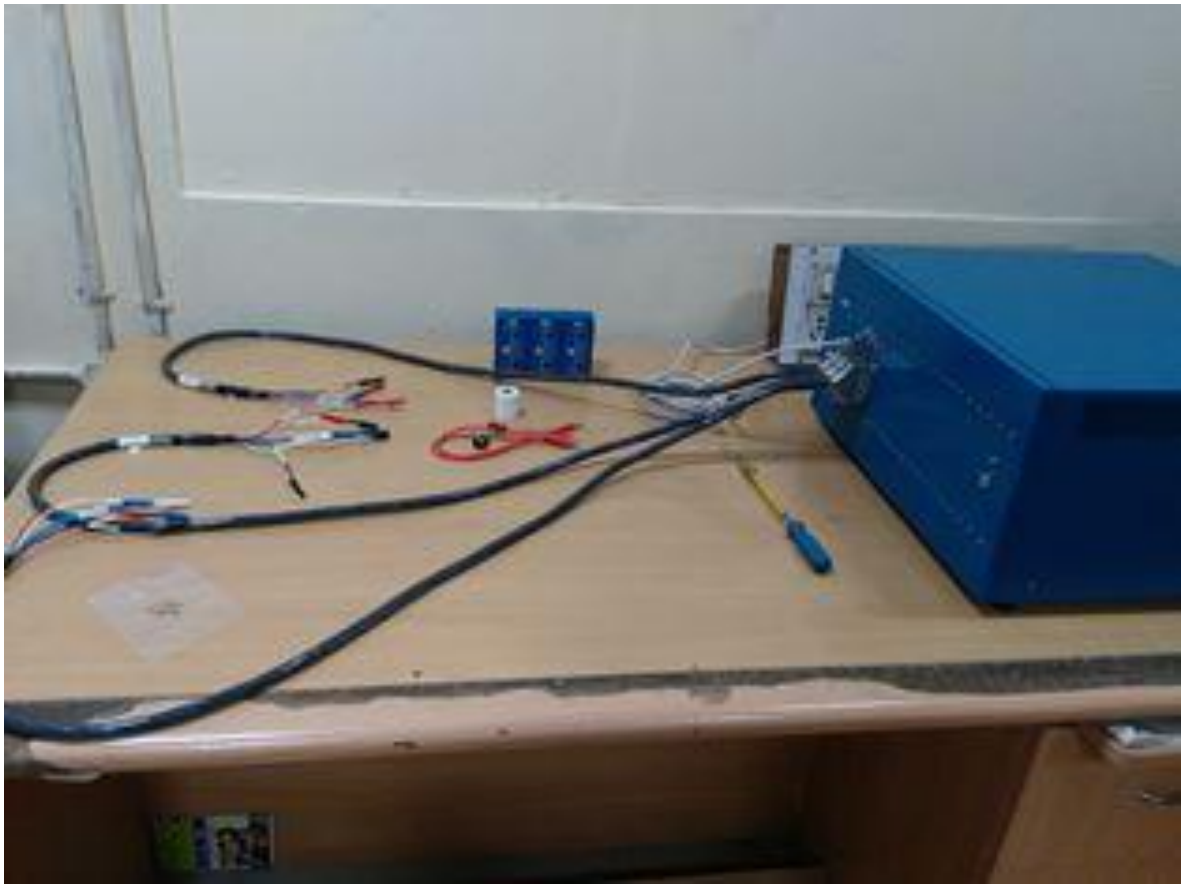

Fig 4.6 Biologic make Potentiostat/Galvanostat/FRA electrochemical analyzer used in the measurement of CV, GCD and EIS data

Chapter-5

Results and Discussions

5.1 X- ray Diffraction Characterization

Fig 5.1 (A) shows XRD pattern of $Li_3V_2(PO_4)_3$/sucrose or (LVP/sucrose) powder, it has been synthesized using sol-gel method. The XRD indicates the proper phase formation of monoclinic structure along with some impurity peaks at angle 22.4^0. Fig 5 (B) indicate the XRD pattern of LVP doped with 1 wt.% MWCNT synthesized by solid state reaction method.

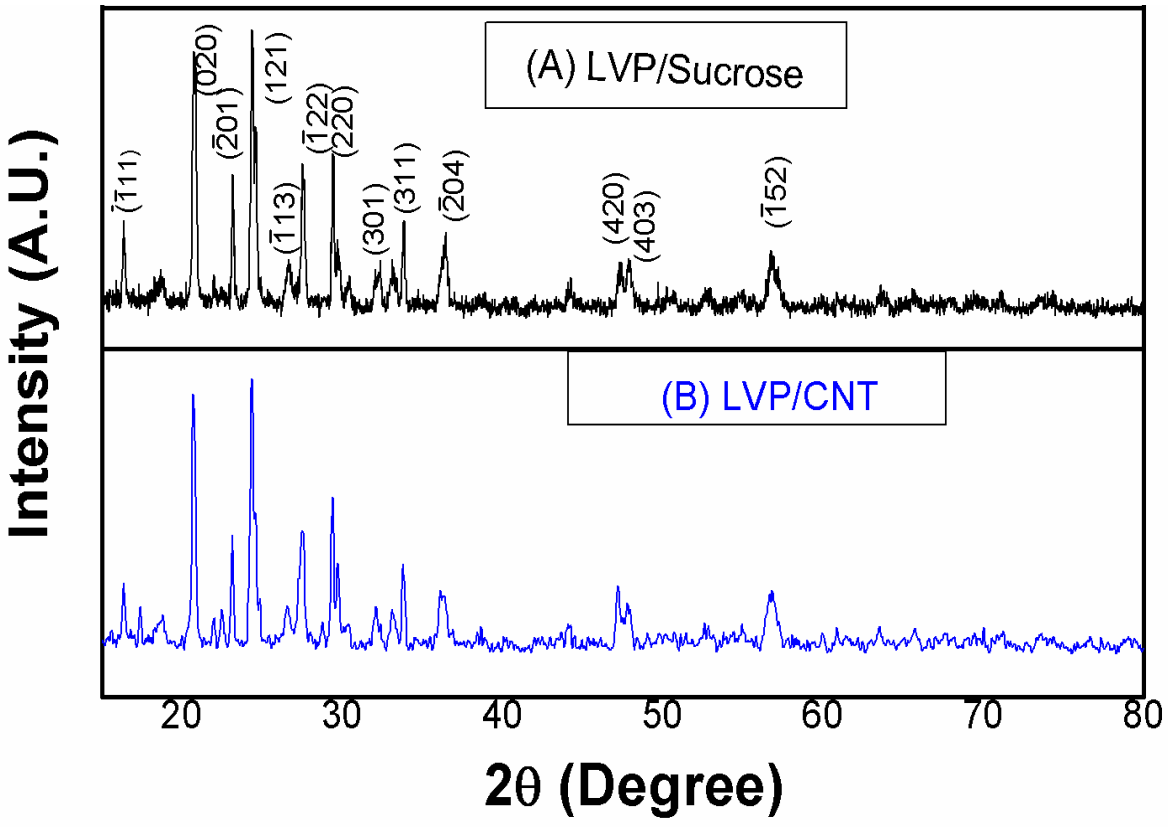

Fig 5.1 XRD pattern of LVP/Sucrose and LVP / MWCNT

XRD pattern of LVP/sucrose and LVP/MWCNT are matched well with the JCPDS data (PDF: 00-47-0107) indicating the formation of monoclinic structure. On the basis of XRD pattern, no extra peak related to carbon is noticed which indicates that the MWCNT does not have a considerable effect on the structure of the sample. To understand it more clearly, diffraction pattern of both the samples were distinguished and their lattice parameters are

given in the Table 5.1 which indicates that the lattice parameter of LVP/MWCNT are smaller than LVP/ sucrose sample and doped MWCNT sample may suppressed the crystal growth of LVP sample.

Table 5.1 The lattice parameter of LVP/ sucrose and LVP/MWCNT composite materials

Samples	a (Å)	b (Å)	c (Å)
LVP/sucrose	8.566	12.039	8.572
LVP/MWCNT	8.520	12.013	8.532

5.2 Scanning Electron Microscope Characterization

Fig 5.2 shows SEM images of both the samples of LVP coated with sucrose and doped with MWCNT using sol gel and solid state reaction route of chemical synthesis respectively. To analyze the particle size, shape and morphology of the samples, scanning electron microscopic (SEM) has been performed. Figure 5.2 (A) and (B) show the SEM images of LVP/ sucrose composition, the irregular shapes and agglomerated morphology with the particle size of about 4-6 µm at two different scales has been observed. Fig 5.2 (C) and (D) show the SEM micrographs of the sample LVP doped with MWCNT using solid state reaction method. It can be seen clearly that the particle size of LVP/MWCNT composition is much smaller as compare LVP/sucrose coated. Hence, average particle size of this LVP/MWCNT composition is observed 1-3 µm. Here, also irregular shape and slightly agglomerated morphology is observed. The agglomeration level of this sample is higher than LVP/ sucrose coated as can be clearly distinguished in SEM images. Mean while, irregular shape of sample shows high extent of homogeneity. It is considered that the synthesized LVP/MWCNT composite material may be suitable for better electrochemical performance as cathode material. As the morphology and particle size have a prominent effect on electro chemical performance of LVP which indicates that LVP/MWCNT shows better performances.

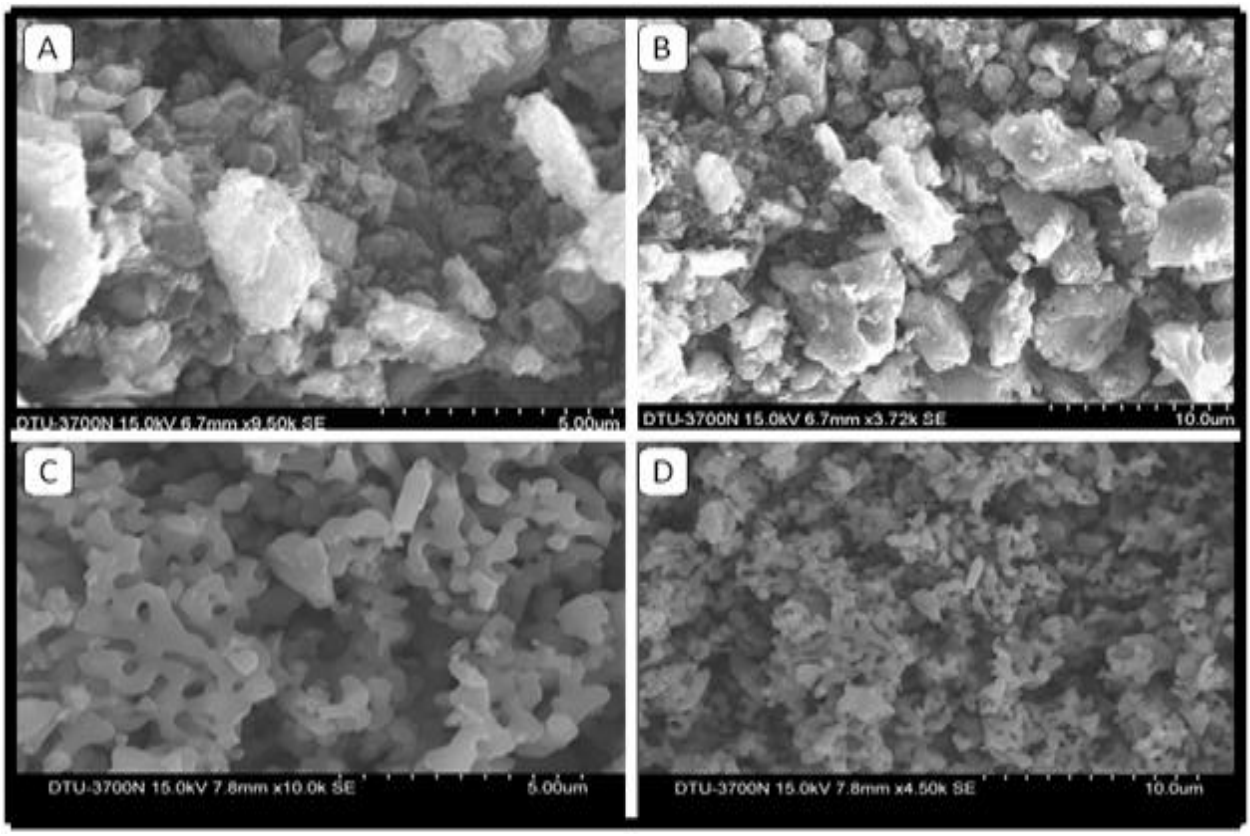

Fig 5.2 SEM images: (A) and (B) LVP/sucrose; C) and (D) LVP/ MWCNT

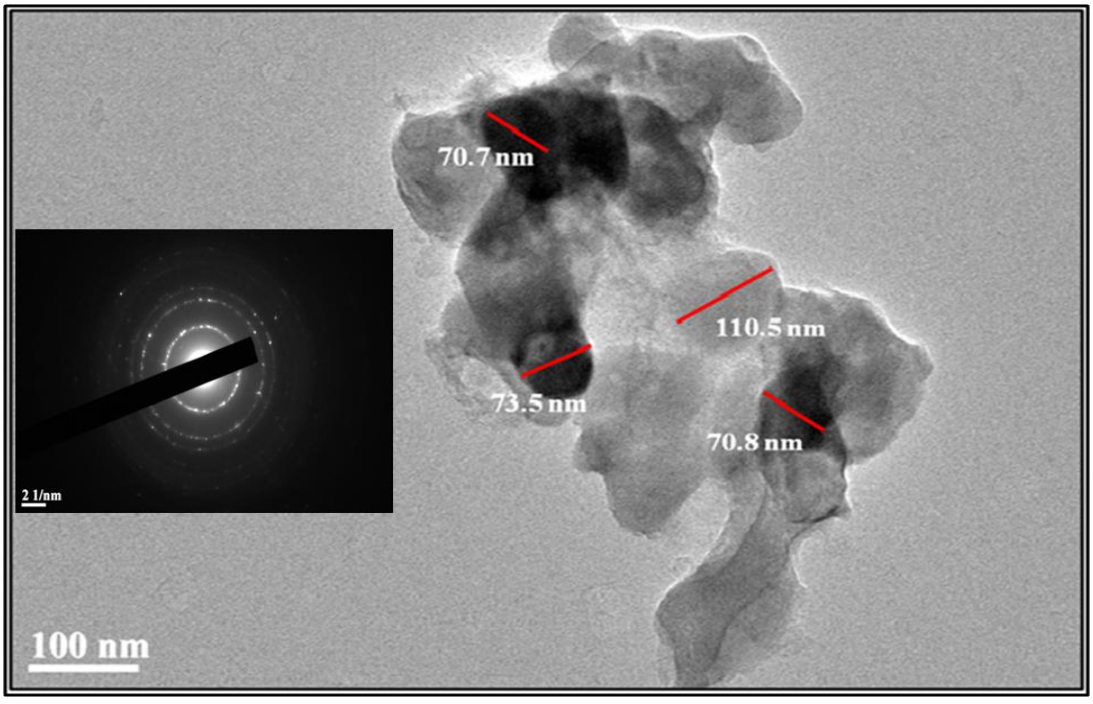

Fig 5.3 TEM image of LVP/sucrose and in inset SAED pattern of LVP/sucrose

Fig 5.3 shows Transmission electron micrograph of prepared sample which represents different particle size and their irregular shape. From TEM image, it is found that the average particle size is approximately 81.4 nm. In inset, Selected Area Electron Diffraction (SAED) pattern have been clearly shown the formation of poly crystalline nature of LVP/sucrose sample. Interplanar distances (d) of particles are approximately 0.332 nm, 0.198 nm and 0.168 nm respectively as can be estimated by SEAD pattern. The circular radius of SEAD pattern shows the parameter "r" which is equal to the inverse of interplanar distance (d).

5.3 Energy Dispersive Spectroscopy (EDS)

Energy-dispersive X-ray spectroscopy (EDS, XEDS or EDX) sometimes called energy dispersive X-ray analysis (EDXA) is an analytical tool used for elemental analysis or chemical characterization of a sample. It depends on an interaction of some source of X-ray excitation and a sample. The main drawback of EDS is that it does not provide any significant peaks for the elements having molecular weight less than 11.

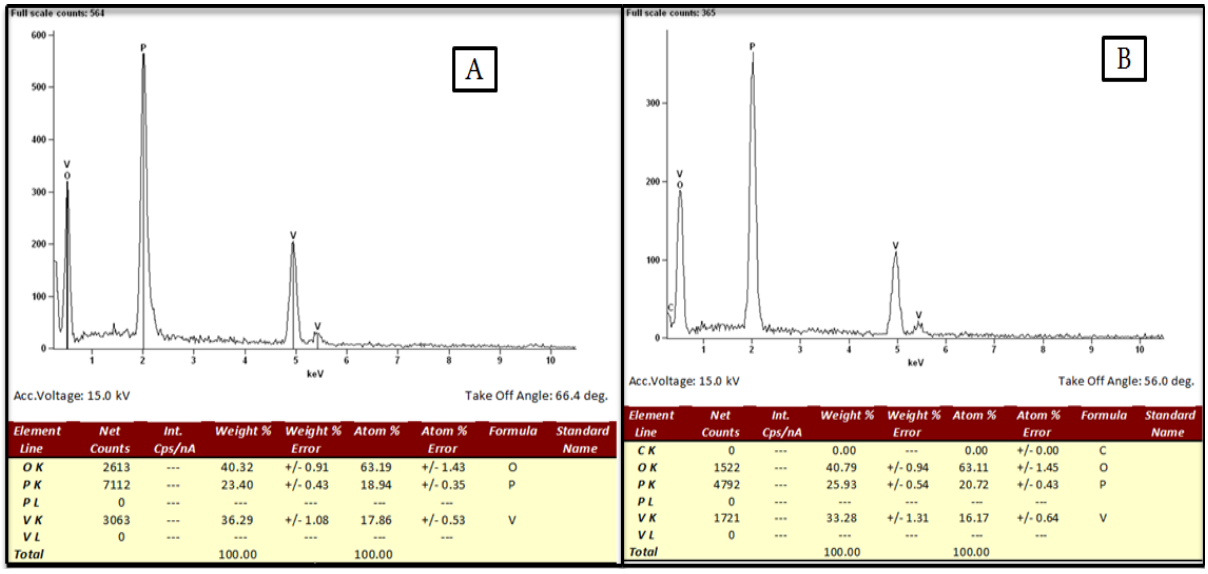

Element Line	Net Counts	Int. Cps/nA	Weight %	Weight % Error	Atom %	Atom % Error	Formula	Standard Name
O K	2613	---	40.32	+/- 0.91	63.19	+/- 1.43	O	
P K	7112	---	23.40	+/- 0.43	18.94	+/- 0.35	P	
P L	0	---	---	---	---	---		
V K	3063	---	36.29	+/- 1.08	17.86	+/- 0.53	V	
V L	0	---	---	---	---	---		
Total			100.00		100.00			

Element Line	Net Counts	Int. Cps/nA	Weight %	Weight % Error	Atom %	Atom % Error	Formula	Standard Name
C K	0	---	0.00	---	0.00	+/- 0.00	C	
O K	1522	---	40.79	+/- 0.94	63.11	+/- 1.45	O	
P K	4792	---	25.93	+/- 0.54	20.72	+/- 0.43	P	
P L	0	---	---	---	---	---		
V K	1721	---	33.28	+/- 1.31	16.17	+/- 0.64	V	
V L	0	---	---	---	---	---		
Total			100.00		100.00			

Fig 5.4 EDS pattern of LVP/sucrose in A and LVP/MWCNT in B

In case of lithium, the emitted x-ray has very low energy therefore it cannot be detected by the EDS. EDS pattern of LVP/sucrose and LVP/MWCNT was observed at accelerating voltage of 15 KV at take off angle 66.4 degree and 56.0 degree respectively. The peak of V, P and O are clearly visible in the EDS pattern of LVP/sucrose and LVP/MWCNT synthesized by sol-gel and solid state method. Figure 5.5 shows the elemental mapping of LVP/sucrose

and LVP/MWCNT which represents dispersion of elements O, V and P at scaling of 2.5 µm and 25 µm respectively.

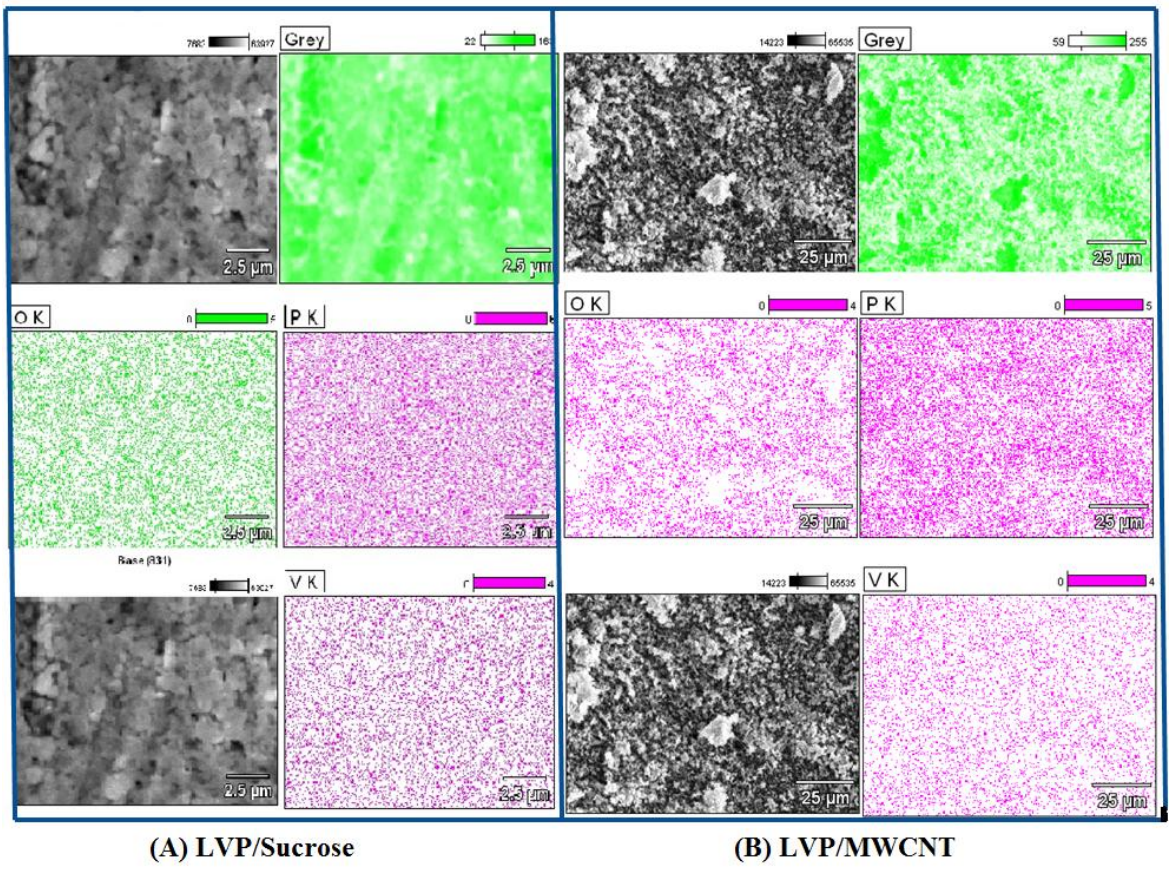

Fig 5.5 Elemental mapping of LVP/ sucrose and LVP/MWCNT

5.4 Fourier Transform Infrared Spectroscopy (FTIR)

Generally, stretching vibrations of $(PO_4)^{3-}$ units and the presence of V–O are the characteristic FTIR options of LVP/ sucrose and LVP/MWCNT compound. Notably, the PO_4 tetrahedral internal modes correspond to the stretching motions and PO_4 external modes correspond to vibrationals and translational motions of P–O bonds. In FTIR, the external modes related to intermolecular vibrations of PO_4 and VO_6 units are found to higher than 400 cm^{-1}. Consequently, stretching vibrations of phosphorus non bridging oxygen bond correspond to the presence of deep singlet at 1045.6 cm^{-1} (Fig 5.6) and therefore the bending vibrations of bilateral and anti symmetric O–P–O bonds are evident from the existence of a doublet at 1220.8 cm^{-1}. Further, presence of a triplet at 635.2, 510.4 and 448 cm^{-1} could also be attributed to the stretching frequency of V–O bonds exist in $Li_3V_2(PO_4)_3$ compound. Interestingly, absence of peaks in 700–900 cm^{-1} region confirms the absence of $(P_2O_7)^{4-}$ and

$(P_3O_{10})^{5-}$ units and thus the presence of $(PO_4)^{3-}$ moiety in $Li_3V_2(PO_4)_3$ is confirmed from FTIR study. Equally presence of meta phosphates containing $R(PO_3)_3$ is additionally not found with the presently synthesized LVP compound, as understood from the absence of peaks between 1240 and 1280 cm^{-1}. Hence, formation of LVP/ sucrose and LVP/MWCNT with preferred native cation surroundings is confirmed by FTIR analysis.

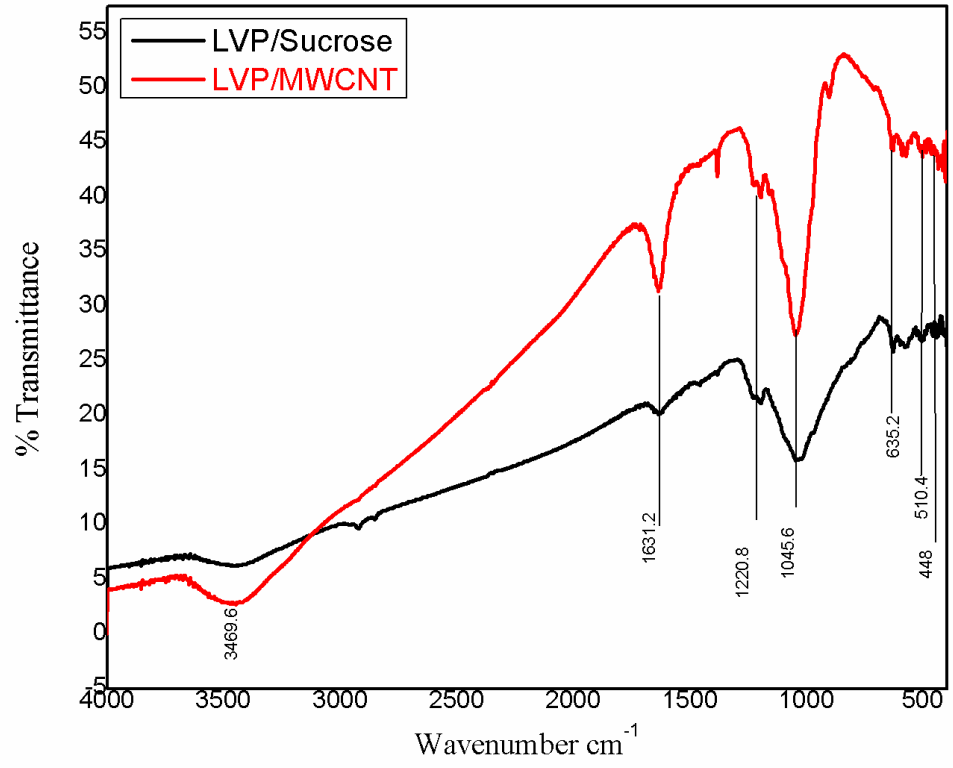

Fig 5.6 Fourier Transform Infrared Spectrum of LVP/ sucrose and LVP/MWCNT

5.5 Electro Chemical Performance

5.5.1 Cyclic Voltammetry (CV)

In order to study the redox reaction mechanism during charging/discharging, CV curves were obtained for the as prepared samples. The scan rate for the CV profiles was 0.05mVs^{-1} in the voltage window of 2.5-4.8 V at room temperature. It can be seen from the CV curves of LVP/sucrose sample that during charging (intercalation), it consists of three sharp peaks at 3.6 V, 3.7 V and 4.1 V which corresponds to the three equations from (1) to (3) while the broad peak above 4.5 V belongs to the oxidation of the electrolyte LiPF6. During discharging (deintercalation) only one broad peak around 3.5 V was observed. It clearly indicates that the redox reaction involved during intercalation/deintercalation of the lithium ion is not

reversible. The intensity of the peak around 4.1 V was found to be highest among all the peaks which show that the lithium ion intercalation at this voltage will be highest.

However, for CNT doped sample, only two peaks was observed during intercalation. The intense peak above 3.75 V accompanied by a shoulder peak has been observed. During deintercalation, a broad peak below 3.5 V is found. These results clearly indicate that the deintercalation voltage shifts to lower values for CNT doped samples as compared to the LVP/sucrose samples.

Overall electro chemical reactions are given below.

Charge:

$$Li_3V_2^{3+}(PO_4)_3 - 0.5Li^+ - 0.5e^- \rightarrow Li_{2.5}V^{3+}V_{½}^{4+}(PO_4)_3 \quad (1)$$

$$Li_{2.5}V^{3+}V_{½}^{4+}(PO_4)_3 - 0.5Li^+ - 0.5e^- \rightarrow Li_2V^{3+}V^{4+}(PO_4)_3 \quad (2)$$

$$Li_2V^{3+}V^{4+}(PO_4)_3 - Li^+ - e^- \rightarrow LiV_2^{4+}(PO_4)_3 \quad (3)$$

$$LiV_2^{4+}(PO_4)_3 - Li^+ - e^- \rightarrow V_2^{4.5+}(PO_4)_3 \quad (4)$$

Discharge:

$$V_2^{4.5+}(PO_4)_3 + 2Li^+ + 2e^- \longrightarrow Li_2V^{3+}V^{4+}(PO_4)_3 \quad (5)$$

$$Li_2V^{3+}V^{4+}(PO_4)_3 + 0.5Li^+ + 0.5e^- \longrightarrow Li_{2.5}V^{3+}V_{½}^{4+}(PO_4)_3 \quad (6)$$

$$Li_{2.5}V^{3+}V_{½}^{4+}(PO_4) + 0.5Li^+ + 0.5e^- \longrightarrow Li_3V_2^{3+}(PO_4)_3 \quad (7)$$

.

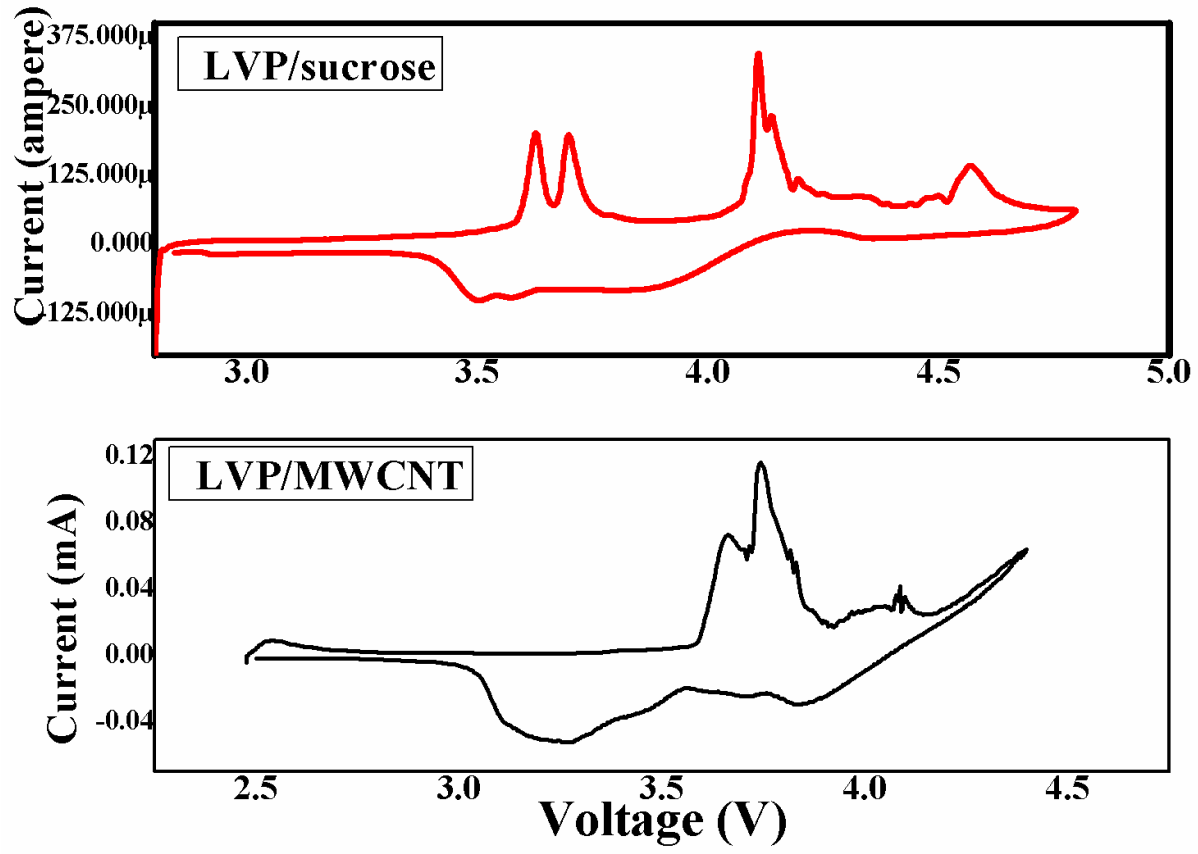

Fig 5.7 CV curve of LVP/ sucrose and LVP/MWCNT at 0.05 mV/s scanning rate in the range of 2.5-4.8 V

5.5.2 Galvanostatic Charge Discharge (GCD)

Fig 5.8 shows first two Galvanostatic charge/discharge (GCD) curves of as synthesized LVP / sucrose and LVP/MWCNT samples in the voltage window of 2.5-4.8 V at the 0.1 C-rate. It can be observed from Fig. 5.8 that the 1st charge curve of the LVP/ sucrose sample consist of three plateaus around 3.6, 4.1and 4.6 V. The length of flat plateau at 4.1 V is more as compared to the plateau at 3.6 V while the plateau at 4.6 V was found to be with little slope. These results indicate that the lithium ion intercalation at these three voltage plateaus follows different mechanism which has been shown in equations (1) to (4). These four equations clearly indicate that every time when a lithium ion moves from cathode to anode during charging, the crystal structure of the cathode material undergoes modifications as oxidation state of vanadium changes. It can be seen from the 1st discharge of LVP/ sucrose sample that during discharging only one plateau with large slope appears which spans a voltage range of 4.2 -3.1 V. It clearly shows that the redox reactions taking place inside the host are not exactly symmetric and reversible as seen from equations (5) to (7). The discharge capacity

for LVP/sucrose is observed about 100 mAh/g and it remains nearly same for the consecutive cycle.

For MWCNT doped LVP/MWCNT sample the charge/discharge curves were found to be more symmetric as compared to LVP/sucrose sample which clearly indicates that the reactions are reversible. Moreover, the plateaus at 3.6 and 4.1 V disappear completely. However, the plateau starts from 4.1 V was found to be steeper as compared to the plateau observed for LVP/ sucrose sample. The discharge capacity was found to be little less for CNT doped LVP and decreases for the consecutive cycle. The discharge capacity was around 90mAh/g for the 1st cycle and 85mAh/g for the 2nd cycle. These results clearly indicate that with CNT doping the multiple plateaus disappears and possibility of structural transformation during charging/discharging for the LVP/MWCNT sample reduced significantly. However, reduction in structural transformation was outshined by decrease in capacity. These results are in well accordance with the CV profiles.

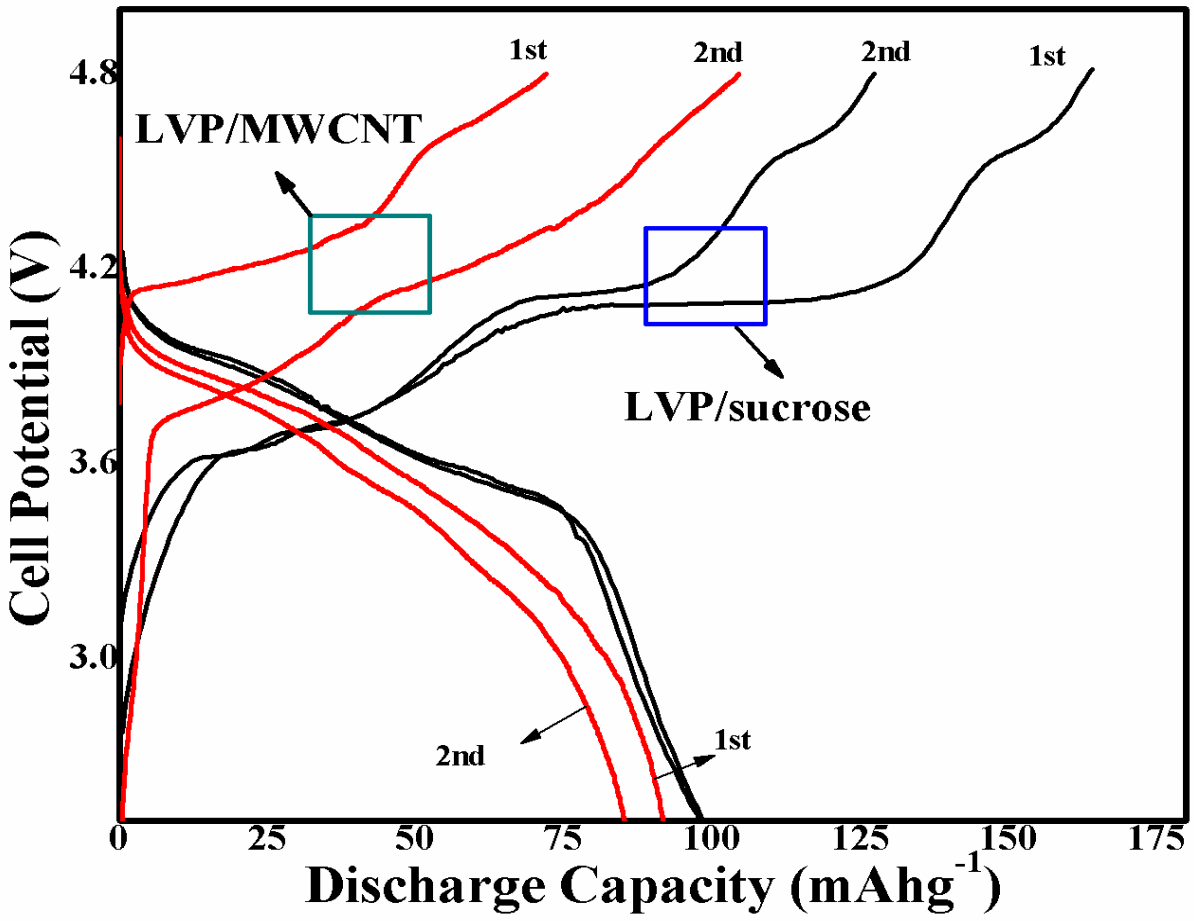

Fig 5.8 Charge discharge profile of LVP and LVP/CNT composition at 0.1C rate in the range of 2.5-4.8 V

5.5.3 Electrochemical Impedance Spectroscopy (EIS) measurements

EIS of the as prepared cells has been shown in Fig. 5.9. It can be seen that the EIS of the samples consists of depressed semicircles in the frequency range of 10 mHz-10 kHz when an AC voltage pulse of amplitude 5mV was applied. The EIS of the cell consist of the electrolyte solution resistance (R_s) which is given by the first intersection of the semicircle close to zero, charge transfer resistance (R_{ct}) which is given by the second intersection of the semicircle at the x-axis and Warburg impedance (Z_w) given by the 45° inclined line. Charge transfer resistance (R_{ct}) attribute the resistance between the electrode and electrolyte interface which is proportional to the diameter of semicircle from first intersection in the low frequency region to the second intersection in high frequency region. Warburg impedance (Z_w) is associated with Li+ diffusion in the bulk solid electrode which is inversely proportional to the slope of inclined line in the low frequency region. From the Fig 5.9 we can clearly deduce that Charge transfer resistance (R_{ct}) of LVP/sucrose and LVP/MWCNT were approximately 100 Ω and 1KΩ, respectively. The charge transfer resistance (R_{ct}) of LVP/CNT was found higher than LVP/sucrose sample.

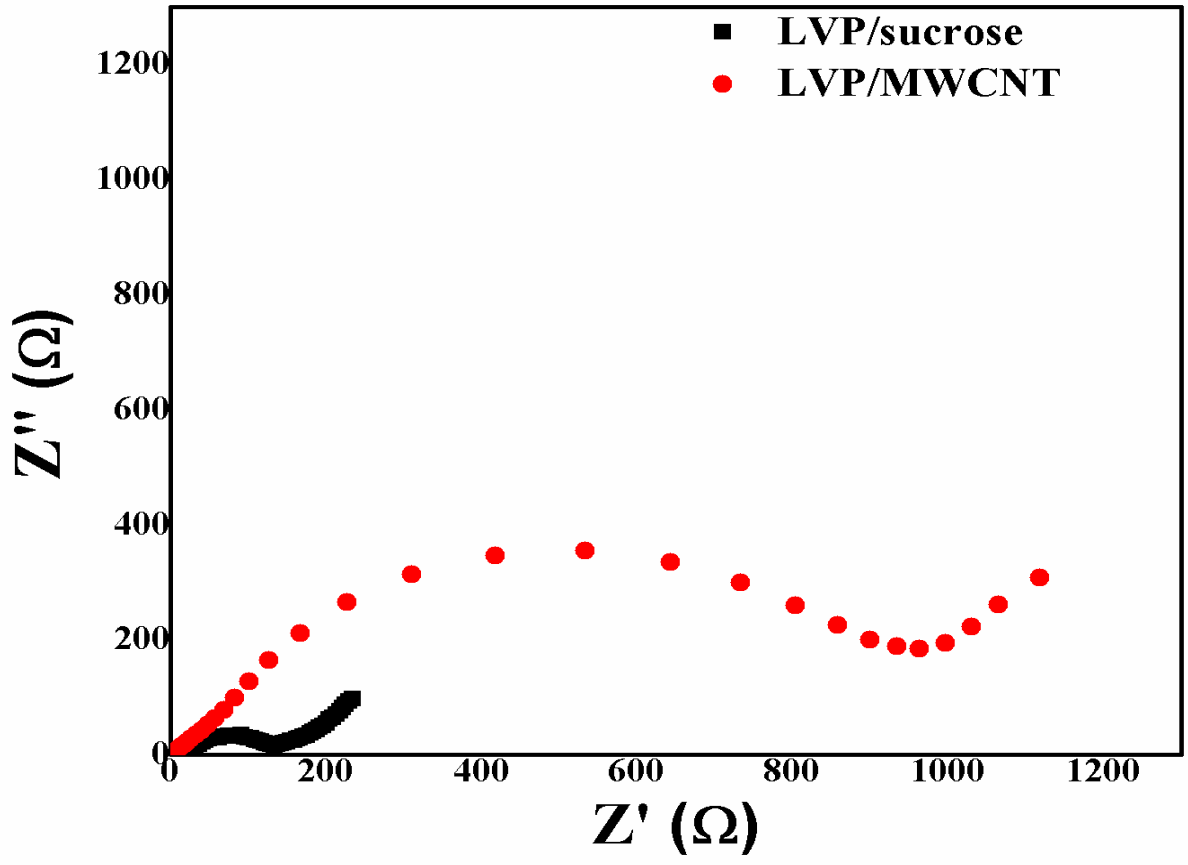

Fig 5.9 Impedance spectra of LVP/sucrose and LVP/MWCNT

5.6 AC CONDUCTIVITY Measurement

AC conductivity of LVP/sucrose samples by sol-gel and LVP/MWCNT composition by solid state route have been measured by LCR meter and Conductivity has been found 5.6×10^{-8} S/cm and 8.3×10^{-9} S/cm, respectively.

Chapter 6

Conclusion

The preparation of LVP by sol-gel and solid state method with sucrose coating and MWCNT doping has been carried out. The calcination temperature and synthesis route have played a significant effect on their morphology, crystal structure and electrochemical behaviour. The XRD pattern of cathode indicates that sucrose coating and MWCNT doping on LVP is not associated to structure collapse and gives a proper phase formation. SEM and TEM result deduce a small and homogenous LVP/sucrose particles having average particle size ~ 81.4 nm (diameter).The initial discharge capacity of LVP/sucrose is 100 mAh/g and that of LVP/MWCNT is 90 mAh/g at 0.1C rate in the range 2.5-4.8 V. Thus according to these electrochemical analysis, LVP/MWCNT shows better properties by reducing the plateau in the discharge curves, indicating that the smaller particle size and relative higher specific surface area will follow easier lithium-ion diffusion. It can be utilized as high rate capability and the process promising for high performance cathode material for lithium-ion batteries. While, LVP/sucrose showing better capacity than LVP/MWCNT, is not found to be potential cathode due to multiple plateaus existing in the discharging curves.

Acknowledgements

Authors are thankful to SERB, Department of Science and Technology (DST), New Delhi for financial support to carry out this work under the project FTP/PS/39/0211.

References

1. "Benjamin Franklin et al.; Leonard W. Labaree, ed., "The Papers of Benjamin Franklin" (New Haven, Connecticut: Yale University Press, 1961) vol. 3, page 352: Letter to Peter Collinson, April 29, 1749. paragraph 18". Franklinpapers.org. Retrieved 2012-08-29.
2. Decker, Franco (January 2005), Electrochemistry Encyclopedia, Case Western Reserve University, Retrieved 2012-11-30.
3. E. Karden, S. Ploumen, B. Fricke, T. Miller, K. Snyder, J. Power Sources 168 (2007) 2.
4. O.Toprakci, H. Toprakci, L. Ji, X. Zhang,, Kona Powder and Particle Journal 28(2010) 50-72.
5. J.M. Tarascon, M. Armand, Nature 414 (6861) (2001) 359.
6. O.Toprakci, H. Toprakci, L. Ji, X. Zhang, Kona Powder and Particle Journal 28(2010) 50-72.
7. Silberberg, M. (2006). Chemistry: The Molecular Nature of Matter and Change, 4th Ed. New York (NY): McGraw-Hill Education. p. 935, ISBN 0077216504.
8. S. Megahed, B. Scrosati, J. Power Sources 51 (1994) 79
9. D. Guyomard, J.M. Tarascon, Adv. Mater. 6 (1994) 408.
10. K. Xu, Chem. Rev. 104 (2004) 4303.
11. Venkataraman, Anuradha, "Pseudocapacitors for Energy Storage" (2015). Dissertations and Theses. Paper 2486.
12. A.Patil, V. Patil, D. W. Shin, J. W. Choi, D.S. Paik, S. J. Yoon, Material Research Bulletin 43 (2008) 1913-1942.
13. M.Y. Saidi, J. Barker, H. Huang, J.L. Swoyer, G. Adamson, Electrochem. Solid State Lett. 5 (2002) A149.
14. Xianhong Rui , Qingyu Yan , Maria Skyllas - Kazacos Tuti Mariana Lim, Journal of Power Sources 258 (2014) 19-38.
15. K. Mizushima, P.C. Jones, P.J. Wiseman, J.B. Goodenough, Mater. Res. Bull. 15(1980) 783..
16. J. Gopalakrishnan, K.K. Rangan, Chem. Mater. 4 (1992) 745.
17. D. Morgan, G. Ceder, M.Y. Saidi, J. Barker, J. Swoyer, H. Huang, G. Adamson, Chem. Mater. 14 (2002) 4684.

18. A.K. Padhi, K.S. Nanjundaswamy, C. Masquelier, J.B. Goodenough, J. Electrochem. Soc. 144 (1997) 2581.
19. S.C. Yin, H. Grondey, P. Strobel, M. Anne, L.F. Nazar, J. Am. Chem. Soc. 125 (2003) 10402.
20. J. Gaubicher, C. Wurm, G. Goward, C. Masquelier, L. Nazar, Chem. Mater.12 (2000 3240.
21. H. Huang, S.C. Yin, T. Kerr, N. Taylor, L.F. Nazar, Adv. Mater. 14 (2002) 1525.
22. M.Y. Saidi, J. Barker, H. Huang, J.L. Swoyer, G. Adamson, J. Power Sources 119 (2003) 266.
23. P. Fu, Y.M. Zhao, Y.Z. Dong, X.N. An, G.P. Shen, J. Power Sources 162 (2006) 651.
24. X.H. Rui, C. Li, C.H. Chen, Electrochim. Acta 54 (2009) 3374.
25. G. Yang, H.D. Liu, H.M. Ji, Z.Z. Chen, X.F. Jiang, Electrochim. Acta 55 (2010) 2951.
26. Q.Q. Chen, J.M. Wang, Z. Tang, W.C. He, H.B. Shao, J.Q. Zhang, Electrochim.Acta 52 (2007) 5251.
27. H.D. Liu, G. Yang, X.F. Zhang, P. Gao, L. Wang, J.H. Fang, J. Pinto, X.F. Jiang, J. Mater. Chem. 22 (2012) 11039.
28. J. Molenda, A. Stoklosa, T. Bak, Solid State Ionics 36 (1989) 53.
29. M.M. Ren, Z. Zhou, Y.Z. Li, X.P. Gao, J. Yan, J. Power Sources 162 (2006) 1357.
30. C.X. Huang, D.D. Chen, Y.Y. Huang, Y.L. Guo, Electrochim. Acta 100 (2013) 1.
31. S. Lee, S.S. Park, J. Phys. Chem. C 116 (2012) 25190.
32. P.P. Prosini, M. Lisi, D. Zane, M. Pasquali, Solid State Ionics 148 (2002) 45.
33. X.H. Rui, D.H. Sim, C. Xu, W.L. Liu, H.T. Tan, K.M. Wong, H.H. Hng, T.M. Lim, Q.Y. Yan, RSC Adv. 2 (2012) 1174.
34. K.M. Shaju, G.V.S. Rao, B.V.R. Chowdari, Electrochim. Acta 48 (2003) 2691.
35. D. Choi, P.N. Kumta, J. Power Sources 163 (2007) 1064.
36. L.J. Wang, H.B. Liu, Z.Y. Tang, L. Ma, X.H. Zhang, J. Power Sources 204 (2012) 197.
37. Le Zhang, Hongfa Xiang, Zhong Li, Haihui Wang School of Chemistry & Chemical Engineering, South China University of Technology, Wushan Road, Guangzhou 510640, China.
38. J.J. Chen, M.J. Vacchio, S.J. Wang, N. Chernova, P.Y. Zavalij, M.S. Whittingham, Solid State Ionics 178 (2008) 1676.

39. Y.Q. Qiao, J.P. Tu, J.Y. Xiang, X.L. Wang, Y.J. Mai, D. Zhang, W.L. Liu, Electrochim. Acta 56 (2011) 4139.
40. G.L. Messing, S.C. Zhang, G.V. Jayanthi, J. Am. Ceram. Soc. 76 (1993) 2707.
41. Y.N. Ko, J.H. Kim, Y.J. Hong, Y.C. Kang, Mater. Chem. Phys. 131 (2011) 292.
42. Y. Zhang, Q.Y. Huo, Y. Lv, L.Z. Wang, A.Q. Zhang, Y.H. Song, G.Y. Li, H.L. Gao, T.C. Xia, H.C. Dong, J. Alloys Compd. 542 (2012) 187.
43. S.Q. Liu, S.C. Li, K.L. Huang, B.L. Gong, G. Zhang, J. Alloys Compd. 450 (2008) 499.
44. J.N. Son, G.J. Kim, M.C. Kim, S.H. Kim, V. Aravindan, Y.G. Lee, Y.S. Lee, J. Electrochem. Soc. 160 (2013) A87.
45. M. Bini, S. Ferrari, D. Capsoni, V. Massarotti, Electrochim. Acta 56 (2011) 2648.
46. Q. Kuang, Y.M. Zhao, X.N. An, J.M. Liu, Y.Z. Dong, L. Chen, Electrochim. Acta 55 (2010) 1575.
47. W.L. Wu, J. Liang, J. Yan, W.F. Mao, J. Solid State Electrochem. 17 (2013) 2027.
48. M.M. Ren, Z. Zhou, Y.Z. Li, X.P. Gao, J. Yan, J. Power Sources 162 (2006) 1357.
49. J. Yan, W. Yuan, Z.Y. Tang, H. Xie, W.F. Mao, L. Ma, J. Power Sources 209 (2012) .
50. C. Deng, S. Zhang, S.Y. Yang, Y. Gao, B. Wu, L. Ma, B.L. Fu, Q. Wu, F.L. Liu, J. Phys. Chem. C 115 (2011) 15048.
51. S. Zhang, Q. Wu, C. Deng, F.L. Liu, M. Zhang, F.L. Meng, H. Gao, J. Power Sources 218 (2012) 56.
52. C.W. Sun, S. Rajasekhara, Y.Z. Dong, J.B. Goodenough, ACS Appl. Mater. Interfaces 3 (2011) 3772.
53. M.M. Ren, Z. Zhou, X.P. Gao, W.X. Peng, J.P. Wei, J. Phys. Chem. C 112 (2008) 5689.
54. T. Jiang, W.C. Pan, J. Wang, X.F. Bie, F. Du, Y.J. Wei, C.Z. Wang, G. Chen, Electrochim. Acta 55 (2010) 3864.
55. W. Yuan, J. Yan, Z.Y. Tang, O. Sha, J.M. Wang, W.F. Mao, L. Ma, J. Power Sources 201 (2012) 301.
56. C. Wang, H.M. Liu, W.S. Yang, J. Mater. Chem. 22 (2012) 5281.
57. X.P. Zhang, H.J. Guo, X.H. Li, Z.X. Wang, L. Wu, Electrochim. Acta 64 (2012) 65.
58. X. Zhang, S.Q. Liu, K.L. Huang, S.X. Zhuang, J. Guo, T. Wu, P. Cheng, J. Solid State Electrochem. 16 (2012) 937.
59. L.L. Ge, C.X. Han, L.P. Ni, J. Zhang, Y.L. Tao, Q.B. Yu, Y.H. Shen, A.J. Xie, L. Zhu, Y.P. Zhang, Solid State Sci. 14 (2012) 864.

60. L.L. Zhang, G. Peng, G. Liang, P.C. Zhang, Z.H. Wang, Y. Jiang, Y.H. Huang, H. Lin, Electrochim. Acta 90 (2013) 433.
61. Https://en.wikipedia.org/wiki/X-ray_crystallography.
62. Https://en.wikipedia.org/wiki/Scanning_electron_microscope.
63. Nanotechnology:Practices and principle by sulebha kulakarni.